Research article

Modeling, stability analysis, and optimal control of a chemostat model for mutualistic bacterial species with leachate recycling

Fawaz K. Alalhareth[1,2,*]**, Ammar R. Aljohani**[3]**, Mohammed H. Alharbi**[3] **and Miled El Hajji**[3,4]

[1] Department of Mathematics, College of Arts and Sciences, Najran University, Najran, Saudi Arabia
[2] Science and Engineering Research Center, Najran University, Najran, Saudi Arabia
[3] Department of Mathematics and Statistics, Faculty of Science, University of Jeddah, P.O. Box 80327, Jeddah 21589, Saudi Arabia
[4] ENIT-LAMSIN, BP. 37, 1002 Tunis-Belvédère, Tunis El Manar University, Tunisia

* **Correspondence:** Email: fkalalhareth@nu.edu.sa.

Abstract: In this paper, we presented a comprehensive mathematical analysis of a chemostat model involving two mutualistic bacterial species competing for nutrients, with the inclusion of leachate recycling. We bridged theoretical ecology and bioreactor design, offering insights into microbial coexistence and system stability. Moreover, we addressed practical challenges in waste-water treatment and bioreactor design by optimizing microbial mutualism and nutrient recycling. The novelty of this study lies in integrating mutualistic interactions, leachate recycling, and optimal control of dilution rates-features seldom combined in chemostat models. We discussed a chemostat model involving two bacterial species that were mutualism competing for two essential nutrients with leachate recycling for one of them. The model was reduced from five dimensions to three, and several equilibrium points were identified: E_0 (extinction of both species), E_1 (extinction of species 2), E_2 (extinction of species 1), and E_{12} (coexistence of both species). The local stability of these equilibria was analyzed. We proved that the coexistence of both species is conditional to some assumptions on the growth rates of species. The coexistence of the two competing bacteria was demonstrated using the theory of uniform persistence applied to the three-variable reduced system. The sensitivity analysis provided valuable insights into the influence of key parameters (e.g., dilution rate and mutualism coefficients) on system dynamics. The optimal control section extends the model's applicability to bioreactor optimization, which is a significant contribution to the field. Several simulations effectively corroborate theoretical findings, illustrating transitions between equilibria and the impact of parameter variations.

Keywords: chemostat; competition; mutualism; coexistence; stability; leachate recirculation; persistence theory; sensitivity analysis; optimal control
Mathematics Subject Classification: 34D23, 37N25, 49J15, 92D25, 93A30

1. Introduction

The study of chemostat models has been a cornerstone in mathematical biology, providing insights into microbial competition, coexistence, and mutualism in controlled environments. In this paper, we build upon a rich body of literature while introducing novel elements such as leachate recycling and mutualistic interactions between bacterial species. Below is a review of key themes and references relevant to this work: The foundational theory of chemostats was established by Smith and Waltman [1] in the theory of the chemostat, which explores the dynamics of microbial competition under constant nutrient supply and dilution. This work laid the groundwork for analyzing steady states, stability, and competitive exclusion. In [2], the authors extend this framework to include mutualistic interactions, adding complexity to the classic competitive exclusion principle. Mutualistic interactions in chemostats have been studied less extensively than competition or predation. The authors draw inspiration from models like those in [3], which analyze microbial food webs in anaerobic digestion, and in [4], which examine bacterial competition in the presence of viruses. These studies highlight how interspecies interactions (e.g., cross-feeding) can stabilize coexistence, a theme central to this paper.

Symbiosis refers to the close association between organisms, with mutualism being a specific form where both species benefit from the interaction [5–7]. Syntrophic interactions, a type of mutualism where at least one organism can live independently, have been extensively examined in chemostat environments [8–10]. Similar well-studied examples is syntrophy can be found in [11–13]. More recent investigations in this area include studies presented in [14–16]. Mutualistic interactions are widespread in nature, such as between plants and seed dispersers [17] or in metabolic cross-feeding, where one bacterium consumes metabolites produced by another [18]. In this study, we model, analyze, and optimize a chemostat system involving two bacteria engaged in metabolic cross-feeding. Our framework captures a fundamental ecological loop, applicable to various systems, including: Detritus recycling by bacteria into nutrients [19], and phytoplankton producing oxygen for bacteria, which in turn supply CO_2 for phytoplankton growth [20]. This generalized structure enables broader ecological and biotechnological applications. The inclusion of leachate recycling is a novel aspect of this work, motivated by applications in waste treatment and bioremediation. Bisi et al. [21] and Laraj et al. [22] provided mathematical frameworks for leachate recirculation in anaerobic systems, demonstrating its role in enhancing nutrient availability and system stability. In this paper, we adapt these ideas to a mutualistic chemostat, showing how recycling influences equilibrium outcomes. We employ tools from dynamical systems theory, such as Lyapunov functions and uniform persistence, to prove coexistence. These methods are well-documented in LaSalle [23] and Smith and Waltman [1]. The stability analysis of equilibria (e.g., E_0, E_{12}) aligns with classical results but extends them to mutualistic systems with recycled nutrients. The optimal control section leverages Pontryagin's Maximum Principle [24] and numerical methods from Lenhart and Workman [25]. In recent years, optimal control methods have been widely applied to complex biological and epidemiological models to balance competing objectives such as disease mitigation and resource allocation. For instance, fractional-order modeling and optimal control approaches were effectively employed in addressing behavioral dynamics in online game addiction based on real data [26]. Similarly, mathematical modeling of infectious diseases, including the competitive transmission of Omicron and Delta COVID-19 strains [27], and the control of mutated Delta strain with imperfect vaccination [28], have utilized optimal control frameworks to capture intervention strategies and system dynamics. Other applications of optimal control to

chemostats (e.g., Fleming and Rishel, [29]) typically focus on single-species systems or predator-prey dynamics. Our innovation lies in optimizing dilution rates for mutualistic species, balancing biomass production and nutrient costs. The sensitivity analysis in the paper echoes techniques used in [3], identifying critical parameters like dilution rates and mutualism coefficients. Numerical simulations validate theoretical predictions, an approach common in modern studies (e.g., [4], on viral dynamics). Sensitivity analysis is performed to understand how the model's behavior changes with variations in the parameters, which is crucial for identifying which parameters have the most significant impact on the system's dynamics, particularly the equilibrium points and their stability.

We discuss a chemostat model with two bacterial species exhibiting mutualistic competition for two nutrients, including leachate recycling for only one substrate. We bridge theoretical ecology and bioreactor design, offering insights into microbial coexistence and system stability. The work provides clear theoretical derivations and numerical validations. The paper is structured into the following sections, each addressing aspects of the chemostat model for mutualistic bacterial species with nutrient recycling. The article moves from theoretical analysis to numerical validation and practical applications. In Section 1, we provided background on chemostat models and their significance in microbial competition and mutualism, reviewed relevant literature, and identified gaps addressed. We combined novel elements like leachate recycling and mutualistic interactions. In Section 2, we described the chemostat model with two bacterial species competing for nutrients. We presented the system of differential equations and assumptions about growth rates and interactions, simplified the model through variable transformations, and proved the existence, non-negativity, and boundedness of solutions. We identified equilibrium points and their biological interpretations and provided lemmas and assumptions for further analysis. In Section 2.1, we analyzed the stability of equilibrium points (E_0, E_1, E_2, E_{12}) using Jacobian matrices and eigenvalue analysis. We stated conditions for stability/instability of each equilibrium. In Section 3, by applying the principle of uniform persistence to the three-variable reduced system, we showed that the two competing bacteria can coexist. In Section 4, we presented MATLAB simulations to validate theoretical findings, including figures showing nutrient and biomass dynamics, phase portraits, and transitions between equilibria. In Section 5, we examined how parameter variations (e.g., dilution rate and mutualism coefficients) affect system behavior. We provided sensitivity coefficients and graphical representations of equilibrium responses. In Section 6, we introduced the optimal control problem with the dilution rate as a control variable, defined the objective functional balancing biomass production and nutrient cost, derived necessary conditions for optimality using the Hamiltonian and adjoint system, explained the characterization of the optimal control, described the forward-backward sweep method for solving the optimal control problem and provided a pseudocode for the algorithm and implementation details. In Section 7, we summarized key findings, including stability and coexistence conditions. We discussed implications for bioreactor design and suggested future research directions.

We introduce several key advancements over the literature, particularly in relation to the foundational work of Smith and Waltman [1] and studies on mutualistic interactions and leachate recycling [14, 21, 22]:

- We formulate a novel chemostat model that integrates two mutualistic bacterial species competing for two distinct essential nutrients, coupled with a leachate recycling mechanism for one substrate, extending classical chemostat frameworks.
- Unlike the researchers in [1] who focused on microbial competition without mutualism or

recycling, we capture mutualistic cross-feeding and nutrient recycling simultaneously with our model, providing richer ecological insights.

- Building on [14] where leachate recycling effects on bacteria with one-way mutualism was investigated, we generalize to mutualistic interactions with bidirectional nutrient exchanges and include optimal control of dilution rates.
- While the researchers in [21, 22] analyzed leachate recirculation in anaerobic digestion, we apply similar concepts innovatively within a bacterial mutualism context and extend the analysis to stability, persistence, sensitivity, and optimal control for bioreactor optimization.
- We rigorously prove coexistence via uniform persistence theory for the reduced system and demonstrate that time-varying dilution rates-derived through Pontryagin's Maximum Principle-significantly enhance biomass production and resource efficiency compared to constant dilution.

These contributions collectively bridge microbial ecology and bioprocess control, offering a comprehensive theoretical and computational framework to guide the management of mutualistic bacterial systems with nutrient recycling.

2. Mathematical model

Consider a chemostat (bioreactor, Figure 1) to which two limiting nutriments are continuously added; one is present in two forms (soluble and insoluble nutriment; N_0^{in} and N_1^{in}), while culture liquid (N_0, N_1, N_2, B_1, B_2) is continuously removed at the same flow rate, D [3]. With general bacterial growth rates and metabolite synthesis that is directly proportional to the bacterial growth, we put forth a mathematical model of two bacteria growing and exchanging nutrients in a chemostat extending the one given in [30]. Following model analysis, conditions are provided in terms of the growth rates and the dilution rate to ascertain the existence and global stability of the equilibria.
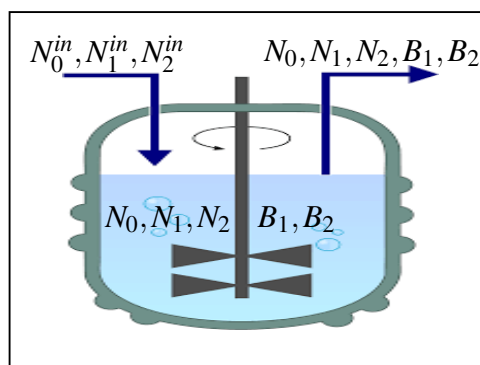

Figure 1. A chemostat is a continuous stirring mechanism (bioreactor) to which two limiting nutriments are continuously added; one is present in two forms (soluble and insoluble nutriment; N_0^{in} and N_1^{in}) is continuously added, while culture liquid (N_0, N_1, N_2, B_1, B_2) and continuously removed at the same flow rate, D.

The model that we propose hereafter is inspired from a previous model proposed in [30] by adding the influence of leachate recirculation as it is applied in [21, 22] with generalized growth rates for both species. Let $N_0(t)$, $N_1(t)$, $N_2(t)$, $B_1(t)$, and $B_2(t)$ stand for the concentrations of insoluble nutriment,

soluble nutriment, bacteria 1, and bacteria 2 inside the chemostat at time t, respectively.

$$
\begin{cases}
\dot{N}_0 &= D(N_0^{in} - N_0) - \delta u N_0, \\
\dot{N}_1 &= D(N_1^{in} - N_1) + \delta u N_0 - \dfrac{f_1(N_1)}{Y_1} B_1 + \beta_2 f_2(N_2) B_2, \\
\dot{N}_2 &= D(N_2^{in} - N_2) - \dfrac{f_2(N_2)}{Y_2} B_2 + \beta_1 f_1(N_1) B_1, \\
\dot{B}_1 &= f_1(N_1) B_1 - D B_1, \\
\dot{B}_2 &= f_2(N_2) B_2 - D B_2.
\end{cases} \tag{2.1}
$$

Model (2.1) describes a controlled, continuous-flow bioreactor (chemostat) inhabited by two species of bacteria that engage in a mutualistic relationship through a process known as metabolic cross-feeding (Figure 1). Furthermore, the system includes a leachate recycling mechanism, a common practice in waste treatment processes like anaerobic digestion, to enhance efficiency. We provide a detailed breakdown of the biological components and processes represented by the variables and equations in model (2.1). In fact, the model tracks the concentrations of five components over time: $N_0(t)$ describes the concentration of an insoluble nutrient (e.g., complex organic matter, solid waste). Bacteria cannot directly consume this; it must first be broken down. $N_1(t)$ describes the concentration of a soluble nutrient that is essential for the growth of bacteria 1. $N_2(t)$ describes the concentration of a different soluble nutrient that is essential for the growth of bacteria 2. $B_1(t)$ describes the biomass concentration of bacterial species 1, while $B_2(t)$ describes the biomass concentration of bacterial species 2. The input concentrations $N_0^{in}, N_1^{in}, N_2^{in}$ are the constant levels of these nutrients in the fresh medium being fed into the chemostat. The system of differential equations (2.1) describes how these five components change over time due to various biological and physical processes (Figure 2).

- $D(N_i^{in} - N_i), i = 1, 2, 3$ describe the chemostat "wash-in/wash-out" terms of nutriments $N_i, i = 1, 2, 3$. Nutrients enter at concentrations N_i^{in} and are washed out at the current concentration N_i.
- The term $\delta u N_0$ represents the hydrolysis or liquefaction of the insoluble nutrient into a soluble form. The parameter δu is the rate constant for this process. This is the first step in the leachate recycling concept, where complex, solid matter is broken down into a bioavailable form, which represents also the soluble product generated from the breakdown of the insoluble nutrient N_0. It directly feeds the pool of N_1.
- $f_i(N_i)/Y_i B_i, i = 1, 2$ describes the consumption of nutriment N_i by bacteria B_i. Bacteria i consumes N_i for growth. The function $f_i(N_i)$ is the growth rate of B_i (e.g., Monod kinetics), Y_i is the yield coefficient (mass of biomass produced per mass of substrate consumed), and this term quantifies the uptake of N_i to support B_i's growth.
- $\beta_i f_i(N_i) B_i$ is the mutualistic input from bacteria B_j for $i, j = 1, 2$ and $i \neq j$. This is the core of the mutualism. As Bacteria i grows (at rate $f_i(N_i)$), it produces N_j as a metabolic byproduct at a rate β_i. This cross-feeding directly benefits bacteria j by supplementing its primary nutrient source.
- Cells are physically removed from the chemostat at the dilution rate D. For a species to survive, its growth rate $f_i(N_i)$ must exceed the dilution rate D; otherwise, it will be washed out.
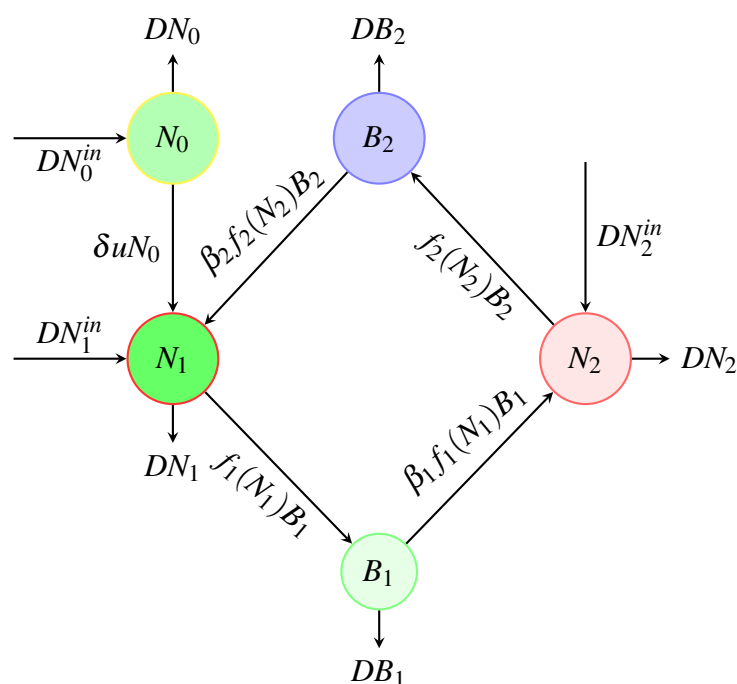
Figure 2. Competition of two species in a chemostat. Circles describe the compartments N_0, N_1, N_2, B_1, and B_2 and the arrows (and labels) correspond to rates of transition between them [3, 31].

Model (2.1) combines three crucial ecological concepts:

(1) Competition for space/resources (implicit): Both species compete indirectly because they share the same physical space (the chemostat) and are subject to the same wash-out rate D. In a classic chemostat without mutualism, this often leads to the competitive exclusion principle, where only one species survives.

(2) Obligate mutualism (syntrophy): The two species have an obligate mutualistic relationship. Each species produces an essential nutrient that the other one needs. This cross-feeding creates a positive feedback loop: more B_1 leads to more N_2, which enables B_2 to grow better, which in turn produces more N_1, further helping B_1. This interaction can stabilize the system and enables coexistence that would be impossible under pure competition.

(3) Nutrient recycling (leachate recycling): The model incorporates a form of nutrient recycling. The insoluble nutrient N_0 is not wasted but is continuously broken down ($\delta u N_0$) and fed back into the soluble nutrient pools (N_1 and indirectly N_2), making the system more efficient and robust. This is highly relevant to environmental processes like decomposition in soils or anaerobic digestion in landfills, where complex waste is broken down by a microbial community.

To conclude, the biological background of model (2.1) is a sophisticated representation of a microbial ecosystem where two bacterial species not only compete for survival in a flowing environment but also depend on each other for essential nutrients, all within a system that recycles complex resources to sustain the community. This makes it a powerful framework for understanding and optimizing processes in wastewater treatment, bioremediation, and microbial ecology.

Model (2.1) is simplified, simplifying the analysis while retaining biological relevance. By making the following change of variable, we obtain a more simplified model. Let $n_0 = N_0$, $n_1 = N_1$, $n_2 = N_2$, $n_0^{in} = N_0^{in}$, $n_1^{in} = N_1^{in}$, $n_2^{in} = N_2^{in}$, $b_1 = \dfrac{B_1}{Y_1}$, $b_2 = \dfrac{B_2}{Y_2}$, $\eta_1 = Y_1\beta_1$, and $\eta_2 = Y_2\beta_2$. Then, the model takes the form

$$
\begin{cases}
\dot{n}_0 & = & D(n_0^{in} - n_0) - \delta u n_0, \\
\dot{n}_1 & = & D(n_1^{in} - n_1) + \delta u n_0 - f_1(n_1)b_1 + \eta_2 f_2(n_2)b_2, \\
\dot{n}_2 & = & D(n_2^{in} - n_2) - f_2(n_2)b_2 + \eta_1 f_1(n_1)b_1, \\
\dot{b}_1 & = & (f_1(n_1) - D)b_1, \\
\dot{b}_2 & = & (f_2(n_2) - D)b_2.
\end{cases}
\tag{2.2}
$$

The growth rates f_1 and f_2 are assumed to be non-negative C^1 functions such that $f_1(0) = f_2(0) = 0$. For the rest of the paper, assume that the growth rates f_1 and f_2 satisfy the following assumption:

Assumption 1.   • f_1 and f_2 are increasing functions, satisfying $f_1(0) = f_2(0) = 0$.
• $0 < \eta_1, \eta_2 < 1$.

Equilibrium points are systematically identified and analyzed for local stability using Jacobian matrices and eigenvalue analysis. The use of Lyapunov functions and uniform persistence theory to demonstrate global stability is mathematically sound. Incorporation of leachate recycling and mutualistic interactions adds originality to the classic chemostat framework. The optimal control section extends the model's applicability to bioreactor optimization. MATLAB simulations effectively corroborate theoretical findings, illustrating transitions between equilibria and the impact of parameter variations. Sensitivity analysis provides practical insights into parameter influences on system dynamics.

We start by giving some technical results, an attractive set and the steady states of system (2.2). Model (2.2) of the chemostat is a dynamical system defined for the non-negative cone, for which we recall some fundamental properties (see for instance [1]).

Proposition 1. *One has*

(1) Solutions of system (2.2) are defined for any positive time and stay non-negative and bounded.

(2) The set $\Sigma = \left\{ (n_o, n_1, n_2, b_1, b_2) \in \mathbb{R}_+^5 \mid n_0 + n_1 + n_2 + (1 - \eta_1)b_1 + (1 - \eta_2)b_2 = n_0^{in} + n_1^{in} + n_2^{in} \right\}$ is a positively invariant attractor of any solution of the system (2.2) in the non-negative cone.

Proof. (1) The invariance of $\mathbb{R}_+^5$ is guaranteed by the following facts: $b_i(t) = 0 \Rightarrow \dot{b}_i(t) = 0$ for $i = 1, 2$, $n_0(t) = 0 \Rightarrow \dot{n}_0(t) = Dn_0^{in} > 0$, $n_1(t) = 0 \Rightarrow \dot{n}_1(t) = \delta u n_0 + Dn_1^{in} + \eta_2 f_2(n_2)b_2 > 0$, and $n_2(t) = 0 \Rightarrow \dot{n}_2(t) = Dn_2^{in} + \eta_1 f_1(n_1)b_1 > 0$.
Consider the variable $T(t) = n_0(t) + n_1(t) + n_2(t) + (1 - \eta_1)b_1(t) + (1 - \eta_2)b_2(t) - n_0^{in} - n_1^{in} - n_2^{in}$. If one adds all equations of system (2.2), one obtains the single equation:

$$
\dot{T}(t) = -DT(t),
\tag{2.3}
$$

from which one deduces

$$
n_0(t) + n_1(t) + n_2(t) + (1 - \eta_1)b_1(t) + (1 - \eta_2)b_2(t) = n_0^{in} + n_1^{in} + n_2^{in} + T_0 e^{-Dt}
$$

with
$$T_0 = n_0(0) + n_1(0) + n_2(0) + (1 - \eta_1)b_1(0) + (1 - \eta_2)b_2(0) - n_0^{in} - n_1^{in} - n_2^{in}.$$

Since each term of the sum is non-negative, we deduce that the solution is bounded.

(2) It is a direct consequence of Eq (2.3).

$\square$

Lemma 1. $n_0^* = \dfrac{Dn_0^{in}}{D + \delta u} \in (0, n_0^{in})$ *is the unique solution of the equation*

$$D(n_0^{in} - n_0) - \delta u n_0 = 0 \ . \tag{2.4}$$

Assumption 2. $f_1(n_0^{in} + n_1^{in} + n_2^{in} - n_0^*) > D.$

Lemma 2. *If the function $f_1 : \mathbb{R}_+ \to \mathbb{R}_+$ satisfies Assumptions 1 and 2, then there exists a unique $n_1^* \in (0, n_0^{in} + n_1^{in} + n_2^{in} - n_0^*)$, satisfying*
$$f_1(n_1^*) = D \ . \tag{2.5}$$

Proof. Let $g_1(n_1) = f_1(n_1) - D$. We obtain $g_1(0) = -D < 0$, $g_1(n_0^{in} + n_2^{in} + n_2^{in} - n_0^*) = f_1(n_0^{in} + n_2^{in} + n_2^{in} - n_0^*) - D > 0$ according to Assumption 2. Furthermore, g_1 is a continuous increasing function according to Assumption 1. Then there exists a unique $n_1^* \in (0, n_0^{in} + n_1^{in} + n_2^{in} - n_0^*)$, such that $g_1(n_1^*) = 0$. $\square$

Assumption 3. $f_2(n_0^{in} + n_1^{in} + n_2^{in} - n_0^*) > D.$

Lemma 3. *If the function $f_2 : \mathbb{R}_+ \to \mathbb{R}_+$ satisfies Assumptions 1 and 3, then there exists a unique $n_2^* \in (0, n_0^{in} + n_1^{in} + n_2^{in} - n_0^*)$, satisfying*
$$f_2(n_2^*) = D \ . \tag{2.6}$$

Proof. Let $g_2(n_2) = f_2(n_2) - D$. We obtain $g_2(0) = -D < 0$, $g_2(n_0^{in} + n_2^{in} + n_2^{in} - n_0^*) = f_2(n_0^{in} + n_2^{in} + n_2^{in} - n_0^*) - D > 0$ according to Assumption 3. Furthermore, g_2 is a continuous increasing function according to Assumption 1. Then there exists a unique $n_2^* \in (0, n_0^{in} + n_1^{in} + n_2^{in} - n_0^*)$, such that $g_2(n_2^*) = 0$. $\square$

Let us define $\bar{b}_1 = n_0^{in} + n_1^{in} - n_0^* - n_1^*$, $\bar{n}_2 = n_2^{in} + \eta_1\bar{b}_1$, $\tilde{b}_2 = n_2^{in} - n_2^*$, $\tilde{n}_1 = n_0^{in} + n_1^{in} - n_0^* + \eta_2(n_2^{in} - n_2^*)$, $b_1^* = \dfrac{n_0^{in} + n_1^{in} + \eta_2 n_2^{in} - (n_0^* + n_1^* + \eta_2 n_2^*)}{(1 - \eta_1 \eta_2)}$ and $b_2^* = \dfrac{\eta_1 n_0^{in} + \eta_1 n_1^{in} + n_2^{in} - (\eta_1 n_0^* + \eta_1 n_1^* + n_2^*)}{(1 - \eta_1 \eta_2)}$.

Therefore, we define the four the equilibrium points of system (2.2) on Σ as follows:

$$E_0 = \left(n_0^*, n_1^{in} + n_2^{in} - n_0^*, n_2^{in}, 0, 0\right), \ E_1 = \left(n_0^*, n_1^*, \bar{n}_2, \bar{b}_1, 0\right), E_2 = \left(n_0^*, \tilde{n}_1, n_2^*, 0, \tilde{b}_2\right), E_{12} = \left(n_0^*, n_1^*, n_2^*, b_1^*, b_2^*\right) \ .$$

Note that E_0 reflects the extinction of both species, E_1 reflects the extinction of the second species while the first species is present, and E_2 reflects the extinction of the first species while the second species is present. Finally, E_{12} reflects the coexistence of both species. Assumptions 1 (A1) and 3 ensure that both species can survive in isolation. Assumption 1 (A2) ensures the interaction terms do not destabilize the system.

2.1. Local stability analysis

Theorem 1. *(1) The trivial equilibrium point E_0 exists always. E_0 is stable if $f_1(n_0^{in} + n_1^{in} - n_0^*) < D$ and $f_2(n_2^{in}) < D$. It is unstable if $\max(f_1(n_0^{in} + n_1^{in} - n_0^*), f_2(n_2^{in})) > D$.*

(2) E_1 exists if $f_1(n_0^{in} + n_1^{in} - n_0^*) > D$. E_1 is stable if $f_2(\bar{n}_2) < D$ and it is unstable if $f_2(\bar{n}_2) > D$.

(3) E_2 exists if $f_2(n_0^{in} + n_1^{in} + n_2^{in} - n_0^*) > D$. E_2 is stable if $f_1(\bar{n}_1) < D$ and it is unstable if $f_1(\bar{n}_1) > D$.

(4) E_{12} exists and is unique if $f_1(n_0^{in} + n_1^{in} + n_2^{in} - n_0^*) > D$ and $f_2(n_0^{in} + n_1^{in} + n_2^{in} - n_0^*) > D$. If it exists, E_{12} is always locally asymptotically stable.

E_0 is globally stable only if both species cannot survive ($f_1(\cdot) < D$) and ($f_2(\cdot) < D$). E_1 and E_2 are not globally stable if the other species can invade ($f_1(\cdot) < D$) or ($f_2(\cdot) < D$). E_{12} is likely globally stable under the given assumptions, but a formal proof (e.g., using Lyapunov functions) is needed for confirmation.

Proof. The local stability of each equilibrium point is determined by analyzing the eigenvalues of the Jacobian matrix evaluated at the equilibrium. The Jacobian matrix of the system (2) is given by:

$$J = \begin{pmatrix} -D - \delta u & 0 & 0 & 0 & 0 \\ \delta u & -D - f_1'(n_1)b_1 & \eta_2 f_2'(n_2)b_2 & -f_1(n_1) & \eta_2 f_2(n_2) \\ 0 & \eta_1 f_1'(n_1)b_1 & -D - f_2'(n_2)b_2 & \eta_1 f_1(n_1) & -f_2(n_2) \\ 0 & f_1'(n_1)b_1 & 0 & f_1(n_1) - D & 0 \\ 0 & 0 & f_2'(n_2)b_2 & 0 & f_2(n_2) - D \end{pmatrix}$$

- For the equilibrium E_0: The Jacobian at $E_0 = (n_0^*, n_1^{in} + n_2^{in} - n_0^*, n_2^{in}, 0, 0)$ simplifies to:

$$J(E_0) = \begin{pmatrix} -D - \delta u & 0 & 0 & 0 & 0 \\ \delta u & -D & 0 & -f_1(n_1^{in} + n_2^{in} - n_0^*) & \eta_2 f_2(n_2^{in}) \\ 0 & 0 & -D & \eta_1 f_1(n_1^{in} + n_2^{in} - n_0^*) & -f_2(n_2^{in}) \\ 0 & 0 & 0 & f_1(n_1^{in} + n_2^{in} - n_0^*) - D & 0 \\ 0 & 0 & 0 & 0 & f_2(n_2^{in}) - D \end{pmatrix}.$$

The eigenvalues are given by $X_1 = -D - \delta u < 0$, $X_2 = -D < 0$, $X_3 = -D < 0$, $X_4 = f_1(n_1^{in} + n_2^{in} - n_0^*) - D$, and $X_5 = f_2(n_2^{in}) - D$. Therefore, F_0 is stable if $f_1(n_0^{in} + n_1^{in} - n_0^*) < D$ and $f_2(n_2^{in}) < D$ (both growth rates are below the dilution rate) and both species will wash out of the chemostat over time. Otherwise, it is unstable and at least one species can persist.

- For the equilibrium E_1: The Jacobian at $E_1 = (n_0^*, n_1^*, \bar{n}_2, \tilde{b}_1, 0)$ simplifies to:

$$J(E_1) = \begin{pmatrix} -D - \delta u & 0 & 0 & 0 & 0 \\ \delta u & -D - f_1'(n_1^*)\tilde{b}_1 & 0 & -D & \eta_2 f_2(\bar{n}_2) \\ 0 & \eta_1 f_1'(n_1^*)\tilde{b}_1 & -D & \eta_1 D & -f_2(\bar{n}_2) \\ 0 & f_1'(n_1^*)\tilde{b}_1 & 0 & 0 & 0 \\ 0 & 0 & 0 & 0 & f_2(\bar{n}_2) - D \end{pmatrix}.$$

The eigenvalues are given by $X_1 = -D - \delta u < 0$, $X_2 = -D < 0$, $X_3 = f_2(\bar{n}_2) - D$, and two other eigenvalues those of the following sub-matrix

$$S_1 = \begin{bmatrix} -D - f_1'(n_1^*)\tilde{b}_1 & -D \\ f_1'(n_1^*)\tilde{b}_1 & 0 \end{bmatrix}.$$

Note that $\text{trace}(S_1) = -D - f_1'(n_1^*)\bar{b}_1 < 0$ and $\det(S_1) = Df_1'(n_1^*)\tilde{b}_1 > 0$. Therefore, E_1 is stable if $f_2(\bar{n}_2) < D$. Otherwise, it is unstable.

- For the equilibrium E_2: The Jacobian at $E_2 = (n_0^*, \bar{n}_1, n_2^*, 0, \tilde{b}_2)$ simplifies to:

$$J(E_2) = \begin{pmatrix} -D - \delta u & 0 & 0 & 0 & 0 \\ \delta u & -D & \eta_2 f_2'(n_2^*)\tilde{b}_2 & -f_1(\bar{n}_1) & \eta_2 D \\ 0 & 0 & -D - f_2'(n_2^*)\tilde{b}_2 & \eta_1 f_1(\bar{n}_1) & -D \\ 0 & 0 & 0 & f_1(\bar{n}_1) - D & 0 \\ 0 & 0 & f_2'(n_2^*)\tilde{b}_2 & 0 & 0 \end{pmatrix}.$$

The eigenvalues are given by $X_1 = -D - \delta u < 0$, $X_2 = -D < 0$, $X_3 = f_1(\bar{n}_1) - D$, and two other eigenvalues those of the following sub-matrix

$$S_2 = \begin{bmatrix} -D - f_2'(n_2^*)\tilde{b}_2 & -D \\ f_2'(n_2^*)\tilde{b}_2 & 0 \end{bmatrix}.$$

Note that $\text{trace}(S_2) = -D - f_2'(n_2^*)\bar{b}_2 < 0$ and $\det(S_2) = Df_2'(n_2^*)\tilde{b}_2 > 0$. Therefore, F_2 is stable if $f_1(\bar{n}_1) < D$. Otherwise, it is unstable.

- For the equilibrium E_{12}: The Jacobian at $E_{12} = (n_0^*, n_1^*, n_2^*, b_1^*, b_2^*)$ is:

$$J(E_{12}) = \begin{pmatrix} -D - \delta u & 0 & 0 & 0 & 0 \\ \delta u & -D - f_1'(n_1^*)b_1^* & \eta_2 f_2'(n_2^*)b_2^* & -D & \eta_2 D \\ 0 & \eta_1 f_1'(n_1^*)b_1^* & -D - f_2'(n_2^*)b_2^* & \eta_1 D & -D \\ 0 & f_1'(n_1^*)b_1^* & 0 & 0 & 0 \\ 0 & 0 & f_2'(n_2^*)b_2^* & 0 & 0 \end{pmatrix}.$$

The characteristic polynomial is complex. $J(E_{12})$ admits an eigenvalue $X_1 = -D - \delta u < 0$ and four other eigenvalues those of the following sub-matrix

$$S_{12} = \begin{bmatrix} -D - f_1'(n_1^*)b_1^* & \eta_2 f_2'(n_2^*)b_2^* & -D & \eta_2 D \\ \eta_1 f_1'(n_1^*)b_1^* & -D - f_2'(n_2^*)b_2^* & \eta_1 D & -D \\ f_1'(n_1^*)b_1^* & 0 & 0 & 0 \\ 0 & f_2'(n_2^*)b_2^* & 0 & 0 \end{bmatrix}.$$

The characteristic polynomial is given by

$$P_{12}(X) = X^4 + a_3 X^3 + a_2 X^2 + a_1 X + a_0$$

where

$$\begin{cases} a_3 &= 2D + f_1'(n_1^*)b_1^* + f_2'(n_2^*)b_2^* > 0, \\ a_2 &= D^2 + 2D(f_1'(n_1^*)b_1^* + f_2'(n_2^*)b_2^*) + (1 - \eta_1\eta_2)f_1'(n_1^*)f_2'(n_2^*)b_1^*b_2^* > 0, \\ a_1 &= D^2 f_1'(n_1^*)b_1^* + D^2 f_2'(n_2^*)b_2^* + (2 - \eta_1 - \eta_2)f_1'(n_1^*)f_2'(n_2^*)b_1^*b_2^* > 0, \\ a_0 &= D^2(1 - \eta_1\eta_2)f_1'(n_1^*)f_2'(n_2^*)b_1^*b_2^* > 0. \end{cases}$$

The conditions of the stability according to the Routh-Hurwitz conditions for stability are written as following:

$$a_3 > 0, a_2 > 0, a_1 > 0, a_0 > 0, a_3a_2 - a_1 > 0, a_3a_2a_1 - a_1^2 - a_3^2a_0 > 0.$$

It remains to prove that

$$a_3a_2 - a_1 > 0 \text{ and } a_3a_2a_1 - a_1^2 - a_3^2a_0 > 0.$$

Since we have

$$
\begin{aligned}
a_3a_2 - a_1 &= (2D + f_1'b_1^* + f_2'b_2^*)(D^2 + 2D(f_1'b_1^* + f_2'b_2^*) + (1 - \eta_1\eta_2)f_1'f_2'b_1^*b_2^*) \\
&\quad - (D^2(f_1'b_1^* + f_2'b_2^*) + (2 - \eta_1 - \eta_2)f_1'f_2'b_1^*b_2^*) \\
&= 2D^3 + 4D^2(f_1'b_1^* + f_2'b_2^*) + 2D(1 - \eta_1\eta_2)f_1'f_2'b_1^*b_2^* \\
&\quad + D^2(f_1'b_1^* + f_2'b_2^*) + 2D(f_1'b_1^* + f_2'b_2^*)^2 + (1 - \eta_1\eta_2)(f_1'b_1^* + f_2'b_2')f_1'f_2'b_1^*b_2^* \\
&\quad - D^2(f_1'b_1^* + f_2'b_2^*) - (2 - \eta_1 - \eta_2)f_1'f_2'b_1^*b_2^* \\
&= 2D^3 + 4D^2(f_1'b_1^* + f_2'b_2^*) + 2D(f_1'b_1^* + f_2'b_2^*)^2 \\
&\quad + [(1 - \eta_1\eta_2)(2D + f_1'b_1^* + f_2'b_2^*) - (2 - \eta_1 - \eta_2)]f_1'f_2'b_1^*b_2^*, \\
a_3a_2a_1 - a_1^2 - a_3^2a_0 &= a_1(a_3a_2 - a_1) - a_3^2a_0 \\
&= \left[D^2(f_1'b_1^* + f_2'b_2^*) + (2 - \eta_1 - \eta_2)f_1'f_2'b_1^*b_2^*\right] \\
&\quad \times \left[2D^3 + 4D^2(f_1'b_1^* + f_2'b_2^*) + 2D(f_1'b_1^* + f_2'b_2^*)^2 \right. \\
&\quad \left. + ((1 - \eta_1\eta_2)a_3 - (2 - \eta_1 - \eta_2))f_1'f_2'b_1^*b_2^*\right] \\
&\quad - (2D + f_1'b_1^* + f_2'b_2^*)^2D^2(1 - \eta_1\eta_2)f_1'f_2'b_1^*b_2^*.
\end{aligned}
$$

Let:

$$B = f_1'(n_1^*)b_1^* + f_2'(n_2^*)b_2^*, \quad C = f_1'(n_1^*)f_2'(n_2^*)b_1^*b_2^*.$$

Then,

$$
\begin{aligned}
a_3a_2 &= (2D + B)\left(D^2 + 2DB + (1 - \eta_1\eta_2)C\right) \\
&= 2D^3 + 4D^2B + 2DB^2 + [(1 - \eta_1\eta_2)(2D + B) - (2 - \eta_1 - \eta_2)]C > 0.
\end{aligned}
$$

Note that

$$(1 - \eta_1\eta_2)(2D + B) - (2 - \eta_1 - \eta_2) = 2D(1 - \eta_1\eta_2) + B(1 - \eta_1\eta_2) - 2 + \eta_1 + \eta_2.$$

Since $\eta_1, \eta_2 \in [0, 1)$, $1 - \eta_1\eta_2 > 0$, and for D sufficiently large, this term is positive. Therefore, all terms in $a_3a_2 - a_1$ are positive. Thus,

$$a_3a_2 - a_1 > 0.$$

Now, note that

$$a_3a_2a_1 - a_1^2 - a_3^2a_0 = a_1(a_3a_2 - a_1) - a_3^2a_0.$$

We proved that $a_3a_2 - a_1 = X$ where:

$$X = 2D^3 + 4D^2B + 2DB^2 + [(1 - \eta_1\eta_2)a_3 - (2 - \eta_1 - \eta_2)]C.$$

Also, $a_0 = D^2(1 - \eta_1\eta_2)C$. Then

$$a_1X = \left[D^2B + (2 - \eta_1 - \eta_2)C\right] \times \left[2D^3 + 4D^2B + 2DB^2 + ((1 - \eta_1\eta_2)a_3 - (2 - \eta_1 - \eta_2))C\right]$$

and

$$a_3^2a_0 = (2D + B)^2D^2(1 - \eta_1\eta_2)C.$$

The term a_1X contains higher-order positive terms in D (e.g., $2D^5B$), which dominate the subtraction $a_3^2a_0$ for biologically realistic parameters. Therefore, for $D > 0$ and $\eta_1, \eta_2 \in [0, 1)$:

$$a_3a_2a_1 - a_1^2 - a_3^2a_0 > 0.$$

Since all coefficients a_i are positive due to the system's structure, these inequalities satisfy the Routh-Hurwitz conditions for local stability of the coexistence equilibrium E_{12}. This ensures that the Routh-Hurwitz conditions for stability are satisfied, confirming the local stability of the coexistence equilibrium E_{12}.

$\square$

The local stability's results suggest that the bacteria-mediated interaction enables stable coexistence (E_{12}), which would not occur in the classical competitive exclusion scenario.

3. Global stability

Let us concentrate on the case where the Assumptions 1–3 are satisfied. Global stability ensures that all trajectories of the system converge to an equilibrium point, regardless of initial conditions. For the coexistence equilibrium E_{12}, we proved its local asymptotic stability (Lemma 1) still, we prove its global stability.

3.1. Reduction to a third dimensional dynamics

Lemma 4. *Consider a solution $(n_0, n_1, n_2, b_1, b_2)$ of dynamics (2.2). Let*

$$
\begin{aligned}
\zeta_0 &= n_0 - n_0^*, \\
\zeta_1 &= n_0^{in} + n_1^{in} + n_2^{in} - n_0 - n_1 - n_2 - (1 - \eta_1)b_1 - (1 - \eta_2)b_2 \\
&= n_0^{in} + n_1^{in} + n_2^{in} - n_0^* - n_1 - n_2 - (1 - \eta_1)b_1 - (1 - \eta_2)b_2 - \zeta_0 \,.
\end{aligned}
$$

Then, system (2.2) is equivalent to

$$
\begin{aligned}
\dot{\zeta}_0 &= -(D + \delta u)\zeta_0 \,, \\
\dot{\zeta}_1 &= -D\zeta_1 \,,
\end{aligned}
\tag{3.1}
$$

and

$$
\begin{aligned}
\dot{n}_2 &= D(n_2^{in} - n_2) - f_2(n_2)b_2 + \eta_1 f_1(n_0^{in} + n_1^{in} + n_2^{in} - n_0^* - n_2 - (1 - \eta_1)b_1 - (1 - \eta_2)b_2 - \zeta_0 - \zeta_1)b_1, \\
\dot{b}_1 &= (f_1(n_0^{in} + n_1^{in} + n_2^{in} - n_0^* - n_2 - (1 - \eta_1)b_1 - (1 - \eta_2)b_2 - \zeta_0 - \zeta_1) - D)b_1, \\
\dot{b}_2 &= (f_2(n_2) - D)b_2.
\end{aligned}
\tag{3.2}
$$

The 5D system's (2.2) solutions converge to Σ. It is sufficient to limit the analysis of the dynamics (2.2) onto the set Γ, as our objective is to examine the asymptotic behavior of these solutions. Thus, according to Thieme's findings [32], the trajectories' asymptotic behavior will provide information for the full dynamics (2.2); for other uses, see [2, 33]. The restriction of system (2.2) on Γ leads to

$$
\begin{cases}
\dot{n}_2 = D(n_2^{in} - n_2) - f_2(n_2)b_2 + \eta_1 f_1(n_0^{in} + n_1^{in} + n_2^{in} - n_0^* - n_2 - (1 - \eta_1)b_1 - (1 - \eta_2)b_2)b_1, \\
\dot{b}_1 = (f_1(n_0^{in} + n_1^{in} + n_2^{in} - n_0^* - n_2 - (1 - \eta_1)b_1 - (1 - \eta_2)b_2) - D)b_1, \\
\dot{b}_2 = (f_2(n_2) - D)b_2.
\end{cases}
\tag{3.3}
$$

By considering the reduced dynamics (3.3), the solution (b_1, b_2, p) will be in the three dimensional set

$$\mathscr{S} = \left\{ (n_2, b_1, b_2) \in \mathbb{R}_+^3 : n_2 + (1-\eta_1)b_1 + (1-\eta_2)b_2 \leq n_0^{in} + n_1^{in} + n_2^{in} - n_0^* \right\}.$$

Note that (3.3) is simply system (3.2) by taking $\zeta_0 = \zeta_1 = 0$.

The corresponding equilibrium points of the dynamics (3.3) are F_0, F_1, F_2, and F_{12}, defined as follows:

$$F_0 = \left(n_2^{in}, 0, 0 \right), \ F_1 = \left(\bar{n}_2, \bar{b}_1, 0 \right), F_2 = \left(n_2^*, 0, \tilde{b}_2 \right), F_{12} = (n_2^*, b_1^*, b_2^*) \ .$$

According to Theorem 1, we obtain

Theorem 2. *The equilibria F_0, F_1, and F_2 exist and are unstable, however, F_{12} exists and is locally asymptotically stable.*

The configuration of the equilibria F_0, F_1, F_2, and F_{12} is provided in Figure 3. F_0 corresponds to the case where both species cannot survive. F_1 (respectively, F_2) corresponds to the case where only species 1 (respectively, 2) can persist. F_{12} corresponds to the case where both species will survive.

Figure 3. Steady states configuration restricted to the plane (n_2, b_1, b_2) when $f_1(n_0^{in} + n_1^{in} + n_2^{in} - n_0^*) > D$ and $f_2(n_0^{in} + n_1^{in} + n_2^{in} - n_0^*) > D$. Let F_0, F_1, F_2, and F_{12} to be the restriction of the equilibrium points E_0, E_1, E_2, and E_{12} to the plane (n_2, b_1, b_2). Therefore, F_0, F_1, and F_2 are unstable; however, F_{12} is locally asymptotically stable interior steady state.

Our major results suggest that the bacteria-mediated interaction enables stable coexistence (F_{12}), which would not occur in the classical competitive exclusion scenario. F_{12} is likely globally stable under the given assumptions, but we need to give a formal proof in the following steps for confirmation.

3.2. No periodic trajectories on the boundaries

Let us first prove that there is no possible periodic solutions on the faces of the set $\mathscr{S}$.

- Let (n_2, b_1, b_2) be a solution of (3.3) on the face of $\mathscr{S}$ corresponding to $n_2 = 0$

$$\begin{cases} \dot{b}_1 = (f_1(n_0^{in} + n_1^{in} + n_2^{in} - n_0^* - (1-\eta_1)b_1 - (1-\eta_2)b_2) - D)b_1, \\ \dot{b}_2 = -Db_2. \end{cases} \tag{3.4}$$

defined on $\mathscr{S}_{b_1 b_2}$ given by

$$\mathscr{S}_{b_1 b_2} = \left\{ (b_1, b_2) \in \mathbb{R}_+^2 : \quad (1-\eta_1)b_1 + (1-\eta_2)b_2 \le n_0^{in} + n_1^{in} + n_2^{in} - n_0^* \right\}.$$

The axes $b_1 = 0$ and $b_2 = 0$ are invariant. By transforming the coordination $\rho_1 = \ln(b_1)$ and $\rho_2 = \ln(b_2)$ for $b_1, b_2 > 0$, we obtain a new two dimensional system of ODEs:

$$\begin{cases} \dot{\rho}_1 = h_1(\rho_1, \rho_2) := f_1(n_0^{in} + n_1^{in} + n_2^{in} - n_0^* - (1-\eta_1)e^{\rho_1} - (1-\eta_2)e^{\rho_2}) - D, \\ \dot{\rho}_2 = h_2(\rho_1, \rho_2) := -D. \end{cases} \tag{3.5}$$

Since $\dfrac{\partial h_1}{\partial \rho_1} + \dfrac{\partial h_2}{\partial \rho_2} = -(1-\eta_1)e^{\rho_1} f_1'(n_0^{in} + n_1^{in} + n_2^{in} - n_0^* - (1-\eta_1)e^{\rho_1} - (1-\eta_2)e^{\rho_2}) < 0$ and according to the Dulac criterion [1], the model (3.5) (similarly the model (3.4)) has no periodic orbit leading to no possible trajectory of (3.3) on the face $b_1 b_2$.

- Let (n_2, b_1, b_2) to be a solution of (3.3) on the face of $\mathscr{S}$ corresponding to $b_2 = 0$:

$$\begin{cases} \dot{n}_2 = D(n_2^{in} - n_2) + \eta_1 f_1(n_0^{in} + n_1^{in} + n_2^{in} - n_0^* - n_2 - (1-\eta_1)b_1)b_1, \\ \dot{b}_1 = (f_1(n_0^{in} + n_1^{in} + n_2^{in} - n_0^* - n_2 - (1-\eta_1)b_1) - D)b_1, \end{cases} \tag{3.6}$$

defined on $\mathscr{S}_{n_2 b_1}$ given by

$$\mathscr{S}_{n_2 b_1} = \left\{ (n_2, b_1) \in \mathbb{R}_+^2 : \quad n_2 + (1-\eta_1)b_1 \le n_0^{in} + n_1^{in} + n_2^{in} - n_0^* \right\}.$$

Note that the axis $n_2 = 0$ is repulsive and that the axis $b_1 = 0$ is invariant. By transforming the coordination $\rho_1 = n_2$ and $\rho_2 = \ln(b_1)$ for $n_2, b_1 > 0$, we obtain a new two dimensional system of ODEs:

$$\begin{cases} \dot{\rho}_1 = h_1(\rho_1, \rho_2) := D(n_2^{in} - \rho_1) + \eta_1 f_1(n_0^{in} + n_1^{in} + n_2^{in} - n_0^* - \rho_1 - (1-\eta_1)e^{\rho_2})e^{\rho_2}, \\ \dot{\rho}_2 = h_2(\rho_1, \rho_2) := f_1(n_0^{in} + n_1^{in} + n_2^{in} - n_0^* - \rho_1 - (1-\eta_1)e^{\rho_2}) - D. \end{cases} \tag{3.7}$$

Since $\dfrac{\partial h_1}{\partial \rho_1} + \dfrac{\partial h_2}{\partial \rho_2} = -D - f_1'(n_0^{in} + n_1^{in} + n_2^{in} - n_0^* - \rho_1 - (1-\eta_1)e^{\rho_2})e^{\rho_2} < 0$ and according to the Dulac criterion [1], the model (3.7) (similarly the model (3.6)) has no periodic orbit leading to no possible trajectory of (3.3) on the face $n_2 b_1$.

- Let (n_2, b_1, b_2) to be a solution of (3.3) on the face of $\mathscr{S}$ corresponding to $b_1 = 0$

$$\begin{cases} \dot{n}_2 = D(n_2^{in} - n_2) - f_2(n_2)b_2, \\ \dot{b}_2 = (f_2(n_2) - D)b_2, \end{cases} \tag{3.8}$$

defined on $\mathscr{S}_{n_2 b_2}$ given by

$$\mathscr{S}_{n_2 b_2} = \left\{ (n_2, b_2) \in \mathbb{R}_+^2 : \quad n_2 + (1-\eta_2)b_2 \le n_0^{in} + n_1^{in} + n_2^{in} - n_0^* \right\}.$$

By transforming the coordination $\rho_1 = n_2$ and $\rho_2 = \ln(b_2)$ for $n_2, b_2 > 0$, we obtain a new two dimensional system of ODEs:

$$\begin{cases} \dot{\rho}_1 = & h_1(\rho_1, \rho_2) := D(n_2^{in} - \rho_1) - f_2(\rho_1)e^{\rho_2}, \\ \dot{\rho}_2 = & h_2(\rho_1, \rho_2) := f_2(\rho_1) - D. \end{cases} \tag{3.9}$$

Since $\dfrac{\partial h_1}{\partial \rho_1} + \dfrac{\partial h_2}{\partial \rho_2} = -D - f_2'(\rho_1)e^{\rho_2} < 0$ and according to the Dulac criterion [1], model (3.9) (similarly the model (3.8)) has no periodic orbit, leading to no possible trajectory of (3.3) on the face $n_2 b_2$.

3.3. Persistence

In this section, our goal is to use the model's uniform persistence (3.3) to illustrate how both bacteria coexist. In our situation, all of system's boundary equlibria (3.3) are unstable. Therefore, we use the same proof as the one used in a similar situation in [34] by consistently using the Butler–McGehee lemma [1].

Theorem 3. *Dynamics (3.3) is persistent.*

Proof. Note that the face $b_1 b_2$ is repulsive, and the two faces $n_2 b_1$ and $n_2 b_2$ are invariant. Furthermore, the stable and unstable manifolds of the boundary equilibria are provided in Figure 3. Consider a solution of system (3.3) denoted by $\vec{\theta} = (n_2(t), b_1(t), b_2(t))$ with initial values $\vec{\theta}(0) = (n_2(0), b_1(0), b_2(0))$ provided that $n_2(0) > 0$, $b_1(0) > 0$, and $b_2(0) > 0$. Next, we aim to show by contradiction that the omega limit set contains no points with zero second and third components.

- Let us denote by $\omega(\gamma^+(\vec{\theta}(0)))$ the omega limit set of $\gamma^+(\vec{\theta}(0))$. Assume that $\omega(\gamma^+(\vec{\theta}(0)))$ contains the steady state F_0. The equilibrium F_0 is a saddle point admitting the n_2-axis as the stable manifold $W^s(F_0)$. Therefore, the omega limit set $\omega(\gamma^+(\vec{\theta}(0)))$ cannot be the equilibria F_0. According to Butler–McGehee lemma [1], there exists $\theta^* \neq F_0$ in $\omega(\gamma^+(\vec{\theta}(0))) \cap W^s(F_0)$. Since $W^s(F_0)$ is the n_2-axis, which is unbounded, and because solution of system (3.3) is bounded, then the omega limit set of any trajectory of (3.3) is bounded, so there is a contradiction with the existence of θ^*; and then, $F_0 \notin \omega(\gamma^+(\vec{\theta}(0)))$.
- Suppose that $F_2 \in \omega(\gamma^+(\vec{\theta}(0)))$. The $n_2 b_2$-plane is the stable manifold of F_2 denoted by $W^s(F_2)$. Therefore, the omega limit set $\omega(\gamma^+(\vec{\theta}(0)))$ cannot be the equilibria F_2. According to Butler–McGehee lemma [1], there exists $\theta^* \neq F_2$ inside $\omega(\gamma^+(\vec{\theta}(0))) \cap W^s(F_2) \backslash \{F_2\}$. As $W^s(F_2)$ lies in the $n_2 b_2$-plane, and since the orbit through θ^* is in $\omega(\gamma^+(\vec{\theta}(0)))$ and is unbounded, then there is a contradiction with the fact that F_2 belongs to $\omega(\gamma^+(\vec{\theta}(0)))$.
- Suppose that $F_1 \in \omega(\gamma^+(\vec{\theta}(0)))$. Similarly to F_0 and F_2, there exists $\theta^* \neq F_1$ belonging to $\omega(\gamma^+(\vec{\theta}(0))) \cap W^s(F_1) \backslash \{F_1\}$. Note that the $n_2 b_1$-plane is the stable manifold of F_1 denoted by $W^s(F_1)$. Therefore, the orbit passing through θ^* belonging to $\omega(\gamma^+(\vec{\theta}(0)))$ is unbounded, and this contradicts with the fact that F_1 belongs to $\omega(\gamma^+(\vec{\theta}(0)))$.

Let $\hat{\theta} = (\hat{n}_2(t), \hat{b}_1(t), \hat{b}_2(t))$ with at least one of the second and third components $\hat{b}_1(t)$ and $\hat{b}_2(t)$ be zero, and assume that $\hat{\theta} \in \omega(\gamma^+(\vec{\theta}(0)))$. The orbit through $\hat{\theta}$ belongs to $\omega(\gamma^+(\vec{\theta}(0)))$. Since the orbit should belong to either $b_1 b_2$, $n_2 b_1$, or $n_2 b_2$ faces, it will converge to one of the equilibria F_0, F_1, or F_2 since the possibility of periodic orbits is excluded, contradicting the fact that these equilibria are

unstable. Thus, all components, in particular the second and third components of the solution, are greater than zero, satisfying

$$\liminf_{t \to \infty} b_1(t) > 0 \text{ and } \liminf_{t \to \infty} b_2(t) > 0,$$

and consequently, dynamics (3.3) is persistent. □

3.4. Back to the main dynamics (2.2)

Theorem 4. *Assume that the dynamics (2.2) satisfies Assumptions 1–3, such that $n_0(0) > 0, n_1(0) > 0, n_2(0) > 0, b_1(0) > 0, b_2(0) > 0$ in $\mathbb{R}_+^5$, then both bacteria persist, and $\lim_{t \to +\infty} b_1(t) > 0$ and $\lim_{t \to +\infty} b_2(t) > 0$.*

Proof. Let $(n_0(t), n_1(t), n_2(t), b_1(t), b_2(t))$ be a solution of (2). From (3.1), we deduce that $\zeta_0(t) = \beta_0 e^{-(D+\delta u)t}$, $\zeta_1(t) = \beta_1 e^{-Dt}$ where $\beta_0 = n_0(0) - n_0^*$ and $\beta_1 = n_0^{in} + n_1^{in} + n_2^{in} - n_1(0) - n_2(0) - (1 - \eta_1)b_1(0) - (1 - \eta_2)b_2(0) - n_0(0)$. Therefore, $n_1(t) = n_0^{in} + n_1^{in} + n_2^{in} - n_0^* - n_2(t) - (1 - \eta_1)b_1(t) - (1 - \eta_2)b_2(t) - n_1^{in} + b_1(t) - \beta_0 e^{-(D+\delta u)t} - \beta_1 e^{-Dt}$. Hence $(n_2(t), b_1(t), b_2(t))$ is a solution of the non-autonomous dynamics given hereafter:

$$\begin{cases} \dot{n}_2(t) = D(n_2^{in} - n_2(t)) - f_2(n_2(t))b_2(t) + \eta_1 f_1(n_1(t))b_1(t), \\ \dot{b}_1(t) = (f_1(n_1(t)) - D)b_1(t), \\ \dot{b}_2(t) = (f_2(n_2(t)) - D)b_2(t). \end{cases} \qquad (3.10)$$

The autonomous dynamics (3.10) asymptotically converges to the dynamics (3.3). The phase portrait of the reduced (to Ω) dynamics (3.3) reveals a potential "positive" periodic trajectory and only one locally stable node, with the others being unstable equilibria. Moreover, all solutions in $\mathbb{R}_+^5$ are attracted to Ω. The asymptotic behavior of the trajectory of the dynamics (3.10) is the same as that of the reduced dynamics (3.3), based on Thieme's discoveries [32]. The conclusion is then deduced. □

4. Numerical simulation for the model (2.2)

We design a MATLAB code that implements the chemostat model with two bacterial species exhibiting mutualism, analyzes the stability of equilibrium points, and provides numerical simulations. This code provides a complete implementation of the mathematical model described previously and enables exploration of the system's behavior under different conditions. We implement the ODE system (2.2) from the paper with Monod growth kinetics and compute the Jacobian matrix at each equilibrium, calculate eigenvalues to determine local stability, and implement the stability conditions from Theorem 1. Therefore, we plot the nutrient and bacterial dynamics over time, and a phase portrait. The plots show the system dynamics converging to different equilibria based on parameter values. We use Monod-type functions to model both growth rates:

$$f_1(n_1) = \frac{f_1^{max} n_1}{k_1 + n_1} \text{ and } f_2(n_2) = \frac{f_2^{max} n_2}{k_2 + n_2}$$

where k_1, k_2, f_1^{max}, and f_2^{max} are nonnegative constants.

Figure 4 shows nutrient concentrations (n_0, n_1, n_2) and bacterial biomasses (b_1, b_2) over time for parameter values favoring coexistence. Nutrients stabilize, while both bacteria grow and reach steady state, indicating mutualistic coexistence at dilution rate $D = 1.3125$. Figure 5 provides the phase portrait of n_1 versus b_1 corresponding to Figure 4. The trajectory converges to an equilibrium point, showing a stable relationship between substrate concentration n_1 and bacterial biomass b_1 under the given parameters. Figure 6 shows the nutrient and biomass dynamics at a higher dilution rate $D = 2$. Nutrient concentrations stabilize, but bacterial biomass levels are lower compared to Figure 4, reflecting increased washout pressure on the populations. Figure 7 provides the phase portrait of n_1 versus b_1 for the parameters in Figure 6. The trajectory converges to a different equilibrium with lower biomass levels, consistent with the stronger dilution effect observed. Figure 8 provides the dynamics for reduced maximum growth rate of bacteria 1 ($f_1^{max} = 2$) at $D = 1.5$. Nutrient concentrations remain stable, but species 1 biomass is reduced compared to earlier figures, indicating sensitivity to growth rate changes. Figure 9 provides the phase portrait of n_1 versus b_1 for Figure 8. The bacterial biomass b_1 converges to a lower equilibrium value, reflecting the impact of the reduced growth rate on species 1. Figure 10 provides the nutrient and biomass dynamics with dilution rate increased to $D = 2.45$ and original growth rates. Bacterial biomass is further diminished, with a possibility of approaching washout conditions for one or both species. Figure 11 provides the phase portrait of n_1 versus b_1 for Figure 10. The trajectory approaches a low biomass equilibrium, demonstrating that higher dilution rates reduce bacterial persistence and coexistence stability.
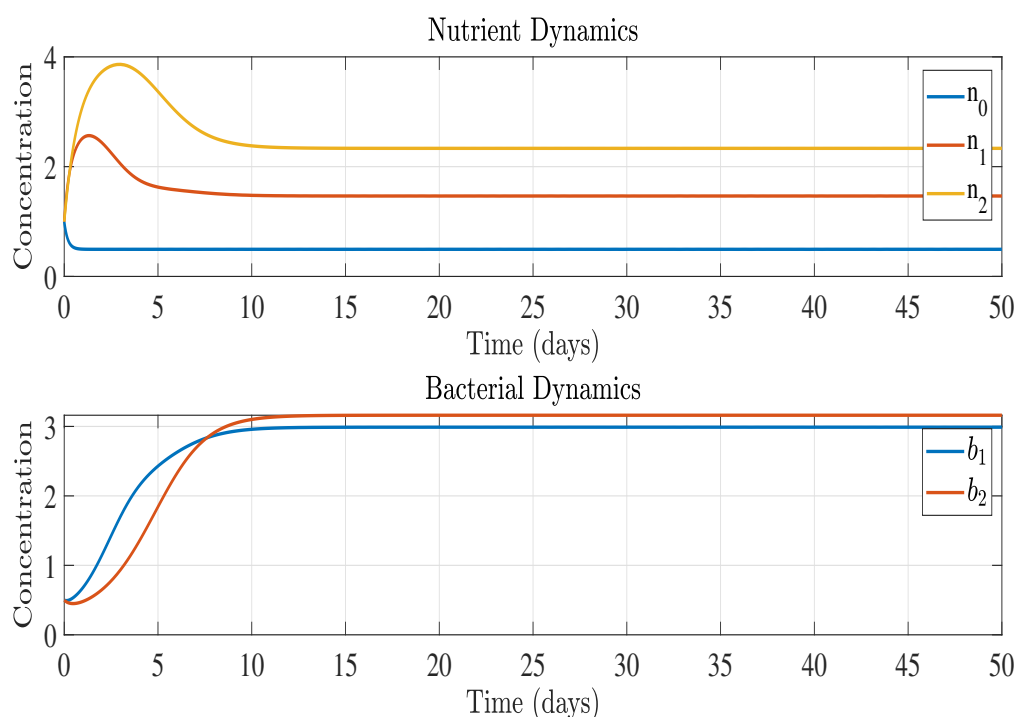

Figure 4. Dynamics of system (2.2). The model parameters are given by: $k_1 = 3$, $k_2 = 3$, $f_1^{max} = 4$, $f_2^{max} = 3$, $n_0^{in} = 2$, $n_1^{in} = 2$, $n_2^{in} = 4$, $\eta_1 = 0.5$, $\eta_2 = 0.3$, $u^0 = 4$ and $D = 1.3125$.
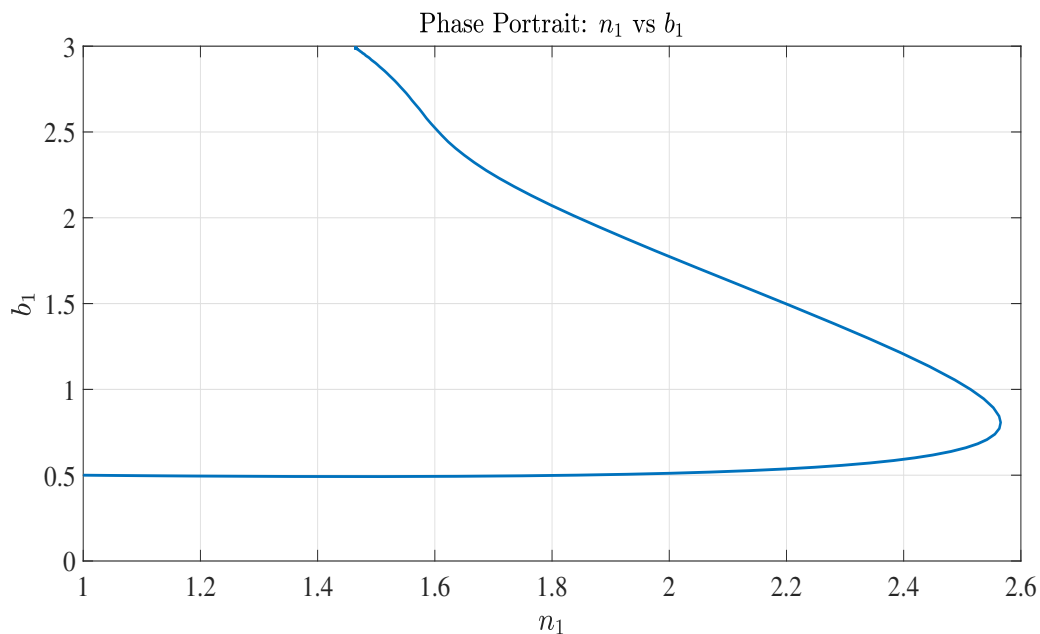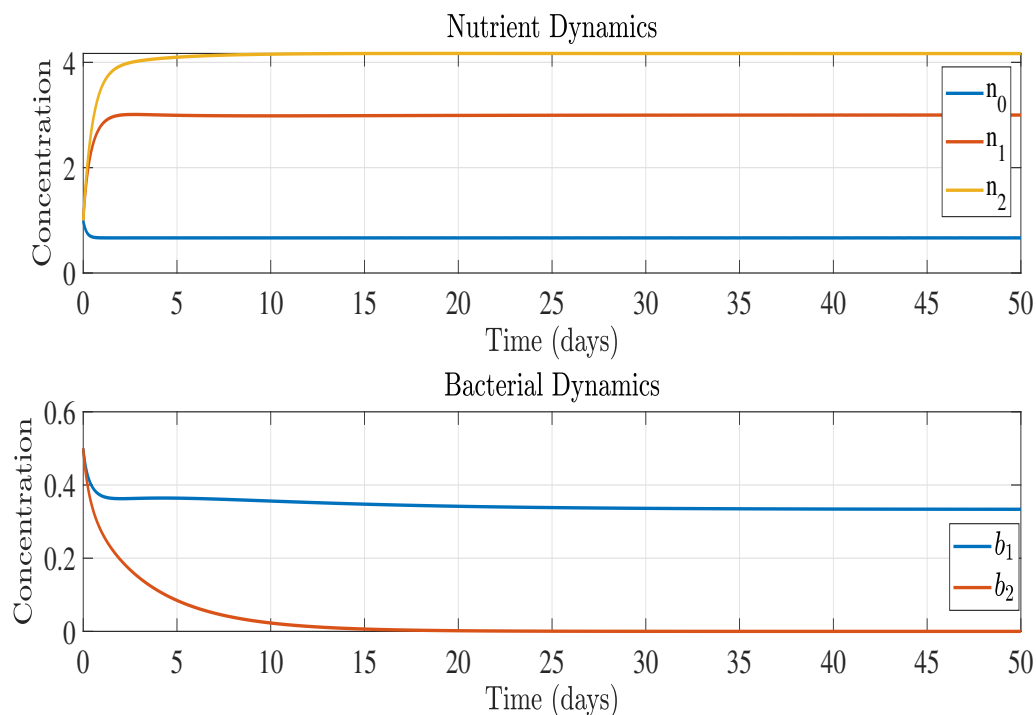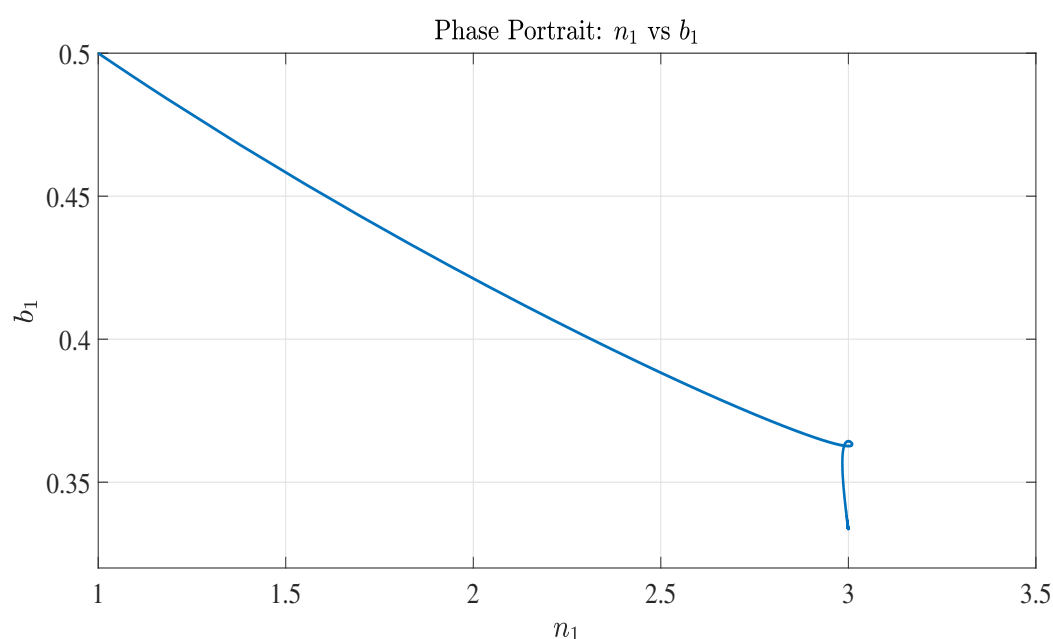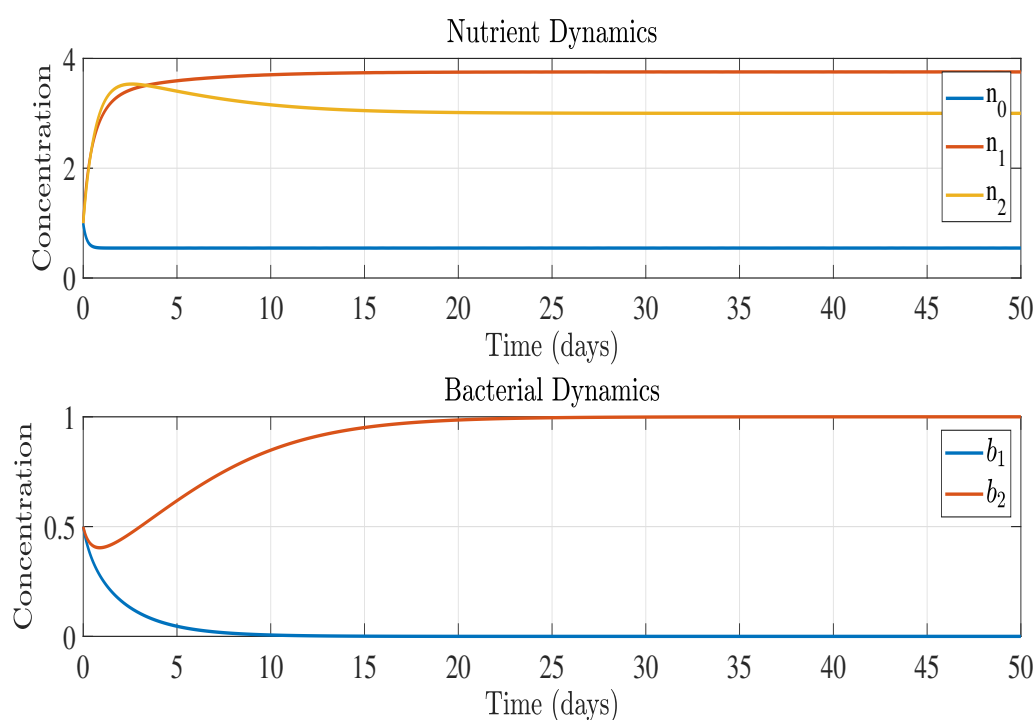
Figure 5. Phase portrait of the variable n_1 vs the variable b_1. The model parameters are given by: $k_1 = 3$, $k_2 = 3$, $f_1^{max} = 4$, $f_2^{max} = 3$, $n_0^{in} = 2$, $n_1^{in} = 2$, $n_2^{in} = 4$, $\eta_1 = 0.5$, $\eta_2 = 0.3$, $u^0 = 4$, and $D = 1.3125$.

Figure 6. Dynamics of system (2.2). The model parameters are given by: $k_1 = 3$, $k_2 = 3$, $f_1^{max} = 4$, $f_2^{max} = 3$, $n_0^{in} = 2$, $n_1^{in} = 2$, $n_2^{in} = 4$, $\eta_1 = 0.5$, $\eta_2 = 0.3$, $u^0 = 4$, and $D = 2$.
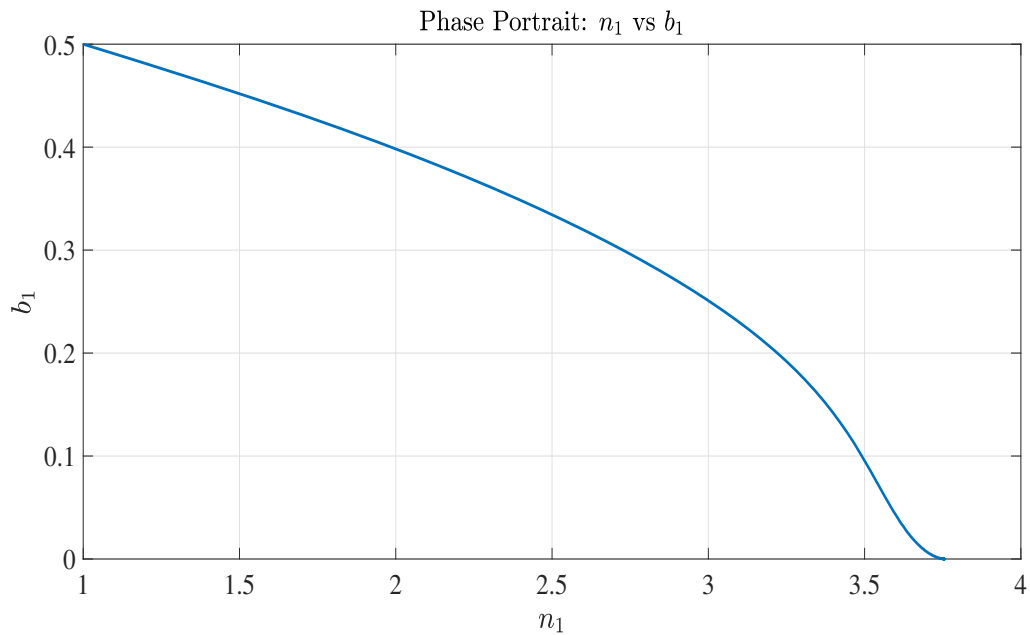
Figure 7. Phase portrait of the variable n_1 vs the variable b_1. The model parameters are given by: $k_1 = 3$, $k_2 = 3$, $f_1^{max} = 4$, $f_2^{max} = 3$, $n_0^{in} = 2$, $n_1^{in} = 2$, $n_2^{in} = 4$, $\eta_1 = 0.5$, $\eta_2 = 0.3$, $u^0 = 4$, and $D = 2$.

Figure 8. Dynamics of system (2.2). The model parameters are given by: $k_1 = 3$, $k_2 = 3$, $f_1^{max} = 2$, $f_2^{max} = 3$, $n_0^{in} = 2$, $n_1^{in} = 2$, $n_2^{in} = 4$, $\eta_1 = 0.5$, $\eta_2 = 0.3$, $u^0 = 4$, and $D = 1.5$.
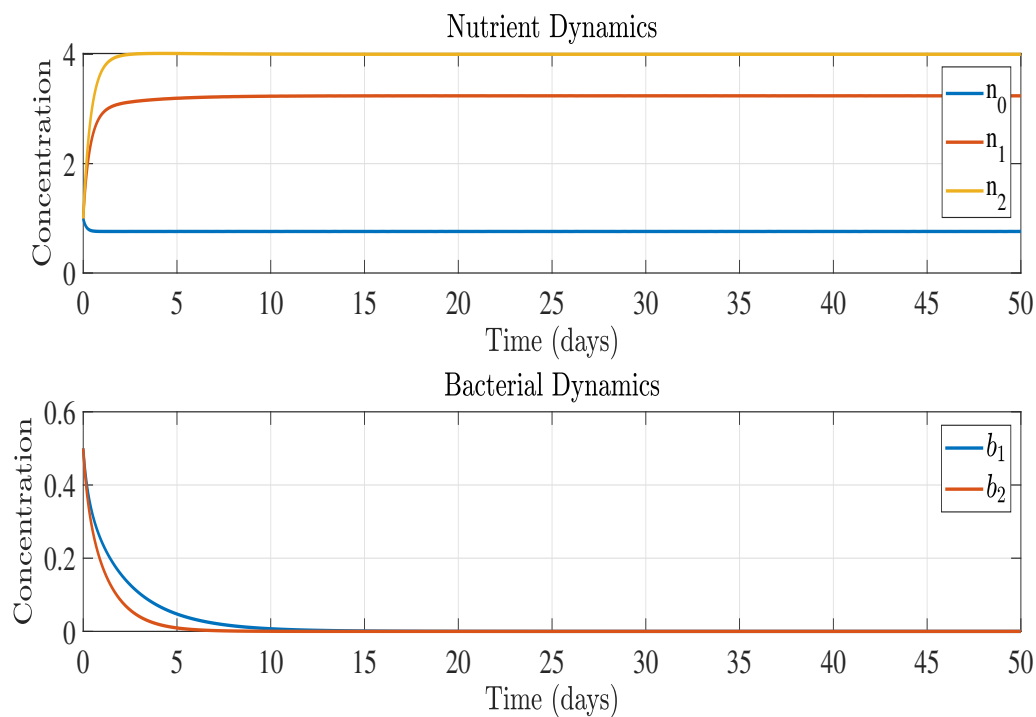
Figure 9. Phase portrait of the variable n_1 vs the variable b_1. The model parameters are given by: $k_1 = 3$, $k_2 = 3$, $f_1^{max} = 2$, $f_2^{max} = 3$, $n_0^{in} = 2$, $n_1^{in} = 2$, $n_2^{in} = 4$, $\eta_1 = 0.5$, $\eta_2 = 0.3$, $u^0 = 4$, and $D = 1.5$.
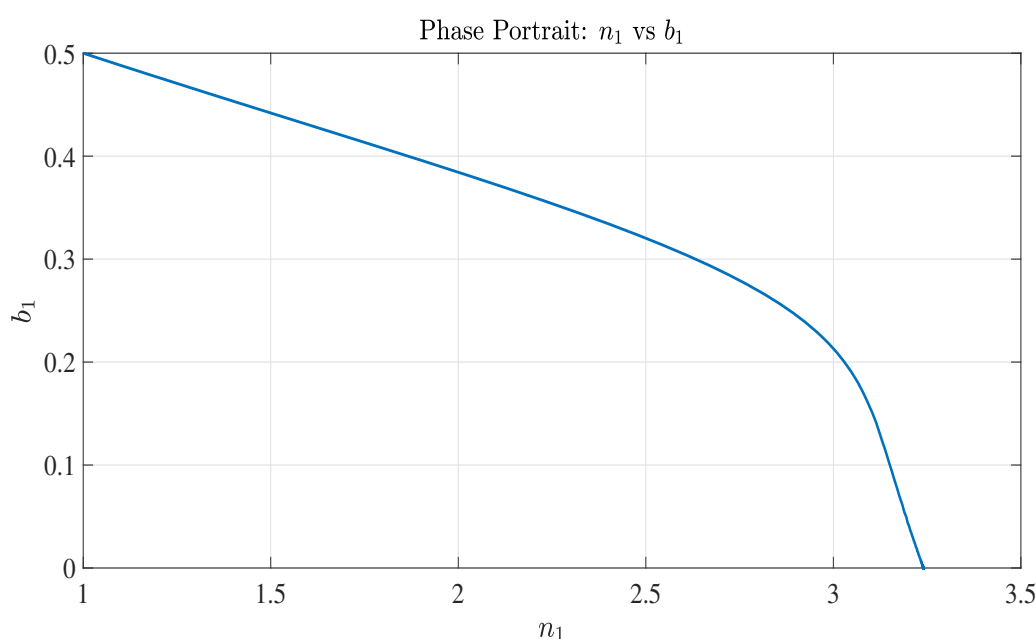

Figure 10. Dynamics of system (2.2). The model parameters are given by: $k_1 = 3$, $k_2 = 3$, $f_1^{max} = 4$, $f_2^{max} = 3$, $n_0^{in} = 2$, $n_1^{in} = 2$, $n_2^{in} = 4$, $\eta_1 = 0.5$, $\eta_2 = 0.3$, $u^0 = 4$, and $D = 2.45$.

Phase Portrait: n_1 vs b_1

Figure 11. Phase portrait of the variable n_1 vs the variable b_1. The model parameters are given by: $k_1 = 3$, $k_2 = 3$, $f_1^{max} = 4$, $f_2^{max} = 3$, $n_0^{in} = 2$, $n_1^{in} = 2$, $n_2^{in} = 4$, $\eta_1 = 0.5$, $\eta_2 = 0.3$, $u^0 = 4$, and $D = 2.45$.

Figures 4–11 collectively illustrate how variations in dilution rate and growth parameters affect nutrient concentrations and bacterial population dynamics, confirming theoretical predictions about stability and coexistence in the chemostat model.

Our numerical simulations focus on the dynamics and stability of the four major equilibria identified in the model with mutualistic bacterial species and leachate recycling. These findings align qualitatively with studies, such as [14, 22, 33], which also investigate mutualistic interactions and nutrient recycling in chemostats but typically consider constant dilution rates without optimal control. Similar to these works, we observe that mutualism and recycling enhance coexistence stability, overcoming classical competitive exclusion scenarios. The equilibrium configurations and sensitivity to dilution rates and mutualism coefficients are consistent with the patterns reported in those studies. However, the introduction of time-varying dilution through optimal control extends the system's dynamic repertoire by enabling adaptive responses to changing system states and objectives. This control flexibility enables trade-offs between maximizing biomass and minimizing nutrient costs, which constant dilution models cannot capture. Consequently, time-varying dilution strategies improve performance, sustain coexistence under a wider range of conditions, and offer practical operational insights for bioreactor management.

5. Sensitivity analysis of the chemostat model with mutualism

In this section, we present a sensitivity analysis of the chemostat model (2.2) with bacterial mutualism. We examine how parameter variations affect system equilibria and stability conditions. This helps us understand how changes in model parameters (e.g., dilution rate D, growth rates f_1, f_2, mutualism coefficients η_1, η_2, and input concentrations n_0^{in}, n_1^{in}, n_2^{in}) affect the stability and behavior

of the system. We discuss how small perturbations in parameters affect equilibrium concentrations. The sensitivity analysis examines the effect of small perturbations in the parameters around their nominal values. The sensitivity of a state variable x with respect to a parameter p is given by the partial derivative $\dfrac{\partial x}{\partial p}$.

The model's key parameters are:

- Dilution rate (D)
- Growth functions ($f_1(n_1), f_2(n_2)$)
- Mutualism coefficients (η_1, η_2)
- Input concentrations ($n_0^{in}, n_1^{in}, n_2^{in}$)

For the equilibrium points E_0, E_1, E_2, and E_{12}, we compute the sensitivity of their components with respect to key parameters such as the dilution rate D, the input concentrations $n_0^{in}, n_1^{in}, n_2^{in}$, and the mutualism coefficients η_1, η_2.

- **Sensitivity of E_0:** The equilibrium $E_0 = (n_0^*, n_1^{in} + n_2^{in} - n_0^*, n_2^{in}, 0, 0)$ depends on D and n_0^{in}. The sensitivity of n_0^* with respect to D is:

$$\frac{\partial n_0^*}{\partial D} = \frac{\delta u n_0^{in}}{(D + \delta u)^2} > 0.$$

  This indicates that n_0^* increases as D increases. Similarly, $\dfrac{\partial n_0^*}{\partial n_0^{in}} = \dfrac{D}{D + \delta u} > 0$, and then n_0^* increases as n_0^{in} increases.

- **Sensitivity of E_1:** The equilibrium $E_1 = (n_0^*, n_1^*, \bar{n}_2, \tilde{b}_1, 0)$ depends on D, n_1^{in}, and η_1. The sensitivity of n_1^* with respect to D is derived from $f_1(n_1^*) = D$:

$$\frac{\partial n_1^*}{\partial D} = \frac{1}{f_1'(n_1^*)} > 0,$$

  since f_1 is increasing. The term $\tilde{b}_1$ is sensitive to n_1^{in}:

$$\frac{\partial \tilde{b}_1}{\partial n_1^{in}} = 1 > 0.$$

- **Sensitivity of E_2:** Similarly, for $E_2 = (n_0^*, \bar{n}_1, n_2^*, 0, \tilde{b}_2)$, the sensitivity of n_2^* with respect to D is:

$$\frac{\partial n_2^*}{\partial D} = \frac{1}{f_2'(n_2^*)} > 0.$$

  The term $\tilde{b}_2$ is sensitive to n_2^{in}:

$$\frac{\partial \tilde{b}_2}{\partial n_2^{in}} = 1 > 0.$$

- **Sensitivity of E_{12}:** The coexistence equilibrium $E_{12} = (n_0^*, n_1^*, n_2^*, b_1^*, b_2^*)$ depends on all parameters. The sensitivities of b_1^* and b_2^* with respect to η_1 and η_2 are particularly important:

$$\frac{\partial b_1^*}{\partial \eta_1} = \frac{\eta_2(n_0^{in} + n_1^{in} + \eta_2 n_2^{in} - n_0^* - n_1^* - \eta_2 n_2^*)}{(1 - \eta_1 \eta_2)^2} > 0,$$

$$\frac{\partial b_2^*}{\partial \eta_2} = \frac{\eta_1(\eta_1 n_0^{in} + \eta_1 n_1^{in} + n_2^{in} - \eta_1 n_0^* - \eta_1 n_1^* - n_2^*)}{(1 - \eta_1 \eta_2)^2} > 0.$$

These results show that the bacterial concentrations b_1^* and b_2^* increase with their respective mutualism coefficients η_1 and η_2, but the positive effect is bounded by the condition $\eta_1 \eta_2 < 1$.

The sensitivity analysis reveals that:

- The dilution rate D is critical for determining whether species can survive. Higher D favors washout.
- The mutualism coefficients η_1, η_2 must satisfy $\eta_1 \eta_2 < 1$ for coexistence. Their values directly influence the equilibrium concentrations of bacteria.
- The input nutrient concentrations n_1^{in} and n_2^{in} are more influential than n_0^{in} for species survival.
- The growth rates f_1, f_2 must exceed D for species to persist, as shown in Assumptions 2 and 3.

The sensitivity analysis highlights the importance of the dilution rate, mutualism coefficients, and nutrient inputs in shaping the chemostat's dynamics. The results align with the theoretical conditions derived for equilibrium stability and coexistence. Numerical methods can further quantify the relative importance of each parameter, guiding experimental design and model refinement.

Figure 12 provides the equilibrium values vs the dilution rate D and the sensitivity coefficients. The top panel (sensitivity coefficients for D) shows:

- How equilibrium concentrations of nutrients (n_0^*, n_1^*, n_2^*) and bacteria (b_1^*, b_2^*) respond to changes in D.
- n_0^* increases with D (higher washout reduces insoluble nutrient conversion).
- n_1^* and n_2^* increase with D due to reduced bacterial consumption at higher dilution.
- b_1^* and b_2^* decrease sharply as D approaches critical values (species wash out when $D > f_1$ or $D > f_2$).
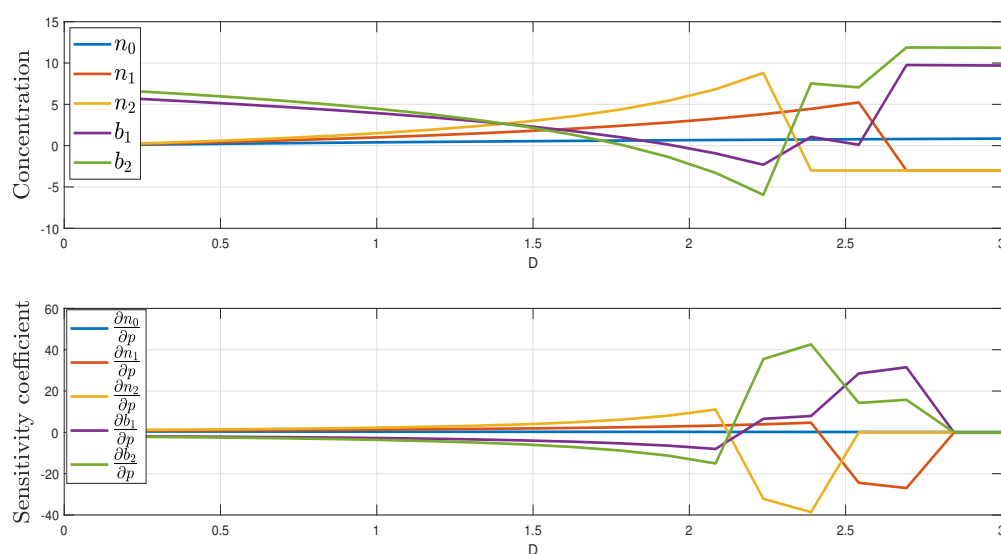

Figure 12. Equilibrium values vs D (down) and sensitivity coefficients for D (up).

However, the bottom panel (Equilibrium Values vs D) illustrates transitions between equilibria:

- For low D, coexistence (E_{12}) dominates.
- Intermediate D leads to single-species equilibria (E_1 or E_2).
- High D results in washout (E_0).

Figure 13 provides the equilibrium values vs mutualism coefficient η_1. The top panel illustrates the sensitivity coefficients for η_1:

- b_1^* increases with η_1 (enhanced mutualism benefits species 1).
- b_2^* decreases slightly due to competition.
- Nutrient levels adjust to balance mutualistic interactions.

However, the bottom panel provides the equilibrium values vs η_1:

- Coexistence is stable only if $\eta_1 \eta_2 < 1$.
- Extreme η_1 values destabilize E_{12}, favoring E_1 or E_2.
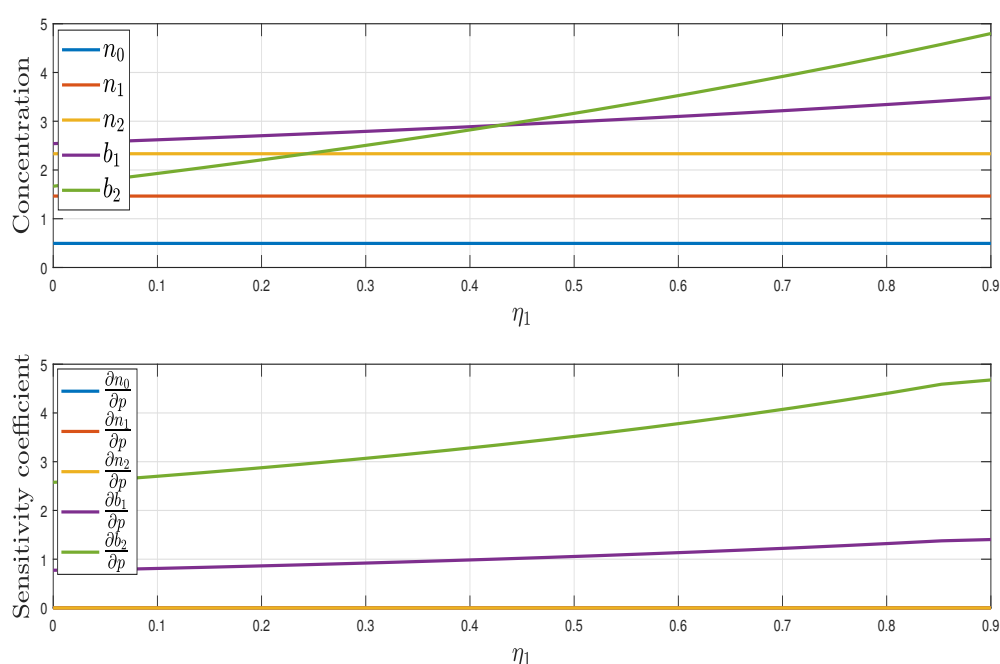

Figure 13. Equilibrium values vs η_1 (down) and sensitivity coefficients for η_1 (up).

Figure 14 provides the equilibrium Values vs Mutualism Coefficient η_2. The top panel illustrates the sensitivity coefficients for η_2:

- Symmetric to Figure 13 but for species 2.
- b_2^* rises with η_2, while b_1^* declines marginally.

However, the bottom panel provides the equilibrium values vs η_2:

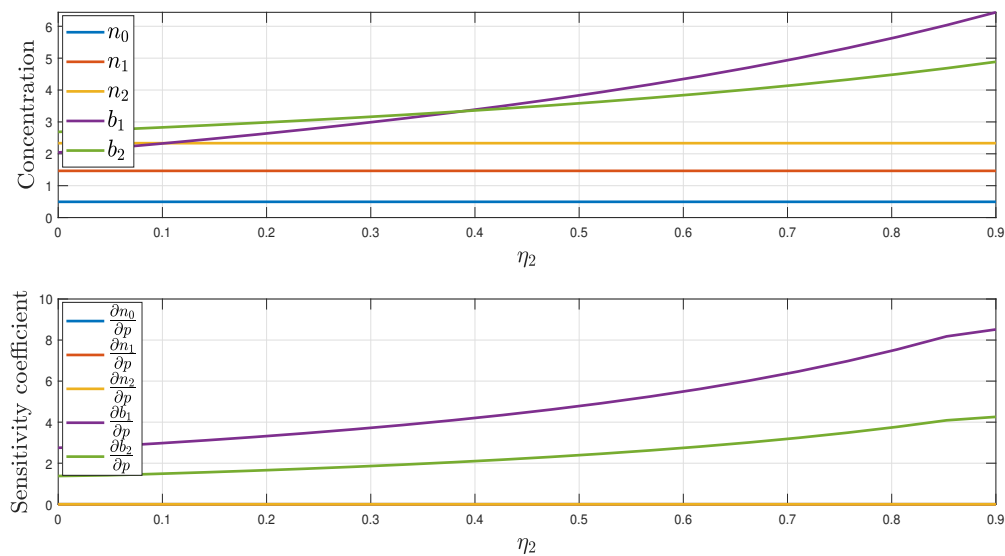- Validates the condition $\eta_1 \eta_2 < 1$ for coexistence.

Figure 14. Equilibrium values vs η_2 (down) and sensitivity coefficients for η_2 (up).

Figures 15–17 provide the equilibrium values vs nutrient inputs $(n_0^{in}, n_1^{in}, n_2^{in})$. The top panel illustrates the sensitivity coefficients:

- n_1^{in} and n_2^{in} have stronger effects on b_1^* and b_2^* than n_0^{in} (direct nutrient dependency).
- n_0^{in} primarily influences n_0^* (insoluble nutrient pool).

However, the bottom panel provides the equilibrium responses:

- Linear increases in b_1^* with n_1^{in} and b_2^* with n_2^{in}.
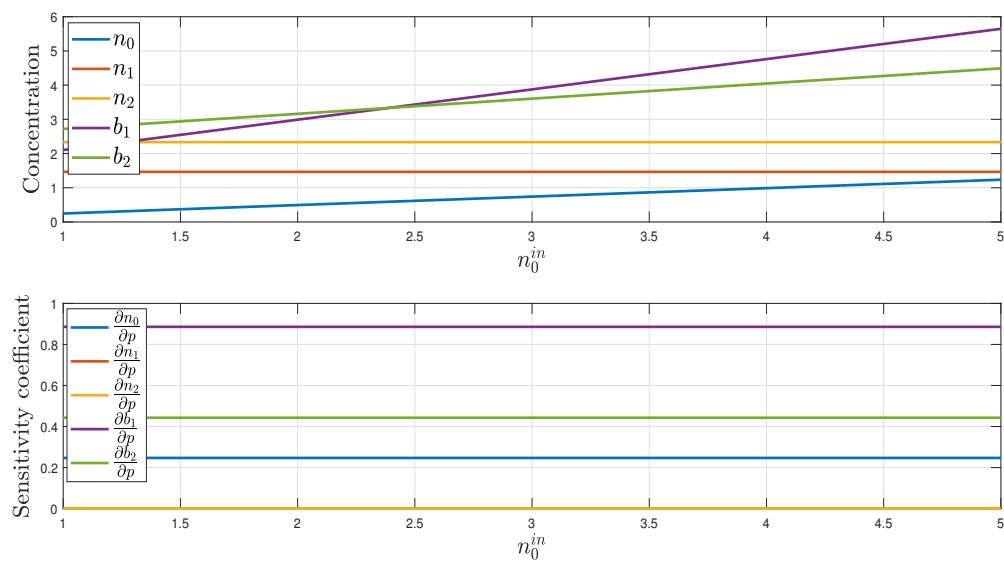- Thresholds exist where additional nutrients no longer boost biomass (growth rate saturation).

Figure 15. Equilibrium values vs n_0^{in} (down) and sensitivity coefficients for n_0^{in} (up).
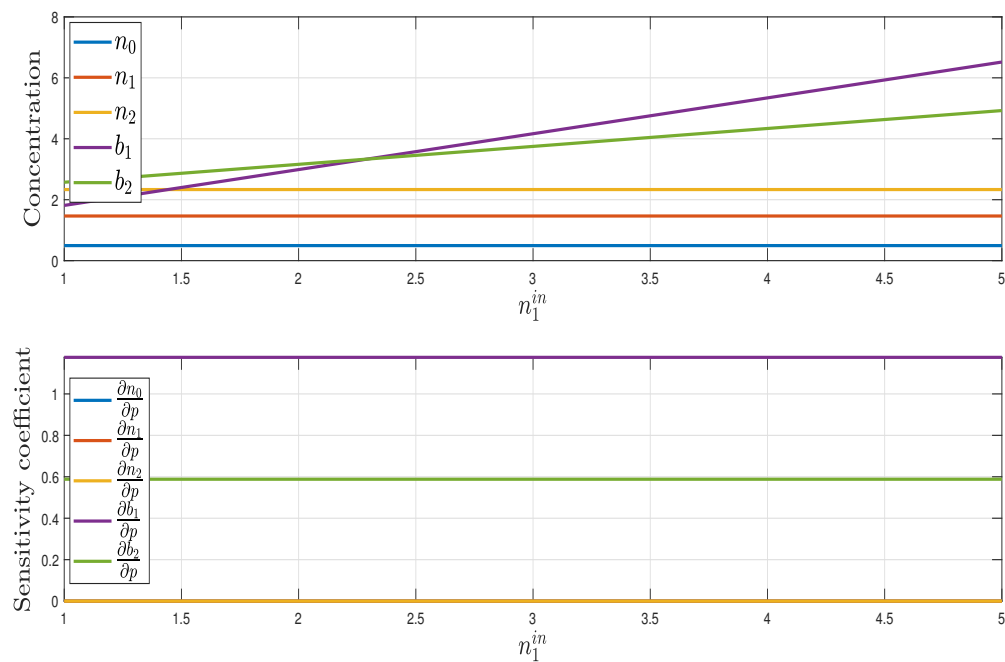
Figure 16. Equilibrium values vs n_1^{in} (down) and sensitivity coefficients for n_1^{in} (up).
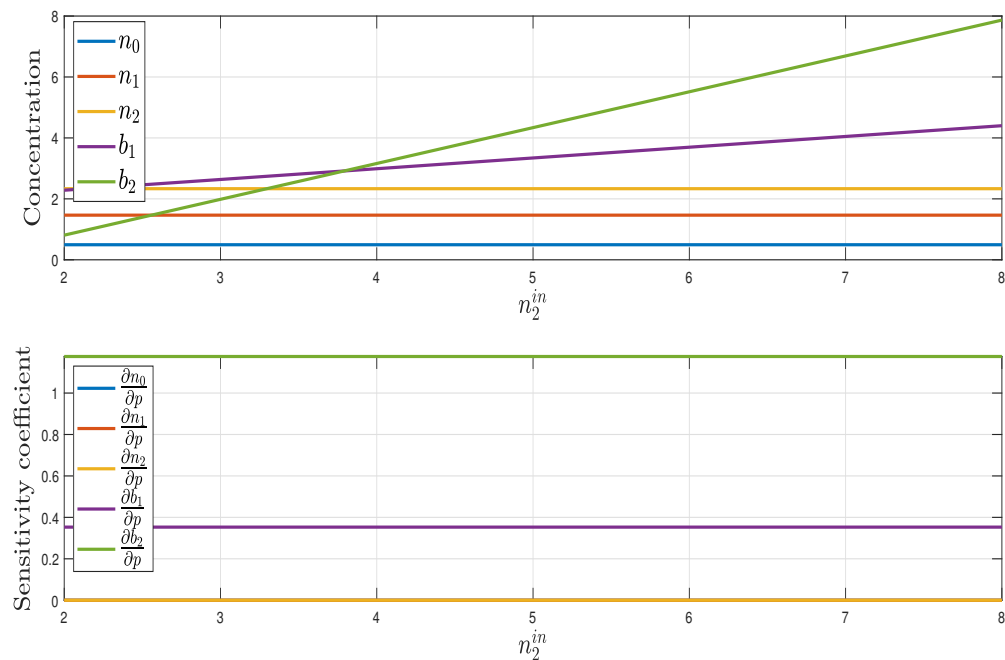

Figure 17. Equilibrium values vs n_2^{in} (down) and sensitivity coefficients for n_2^{in} (up).

Figure 18 provides the local sensitivity of equilibrium components to parameters.

- D is the most influential parameter (determines survival/extinction).
- Mutualism coefficients (η_1, η_2) modulate coexistence stability.
- Nutrient inputs (n_1^{in}, n_2^{in}) are critical for species-specific biomass production.
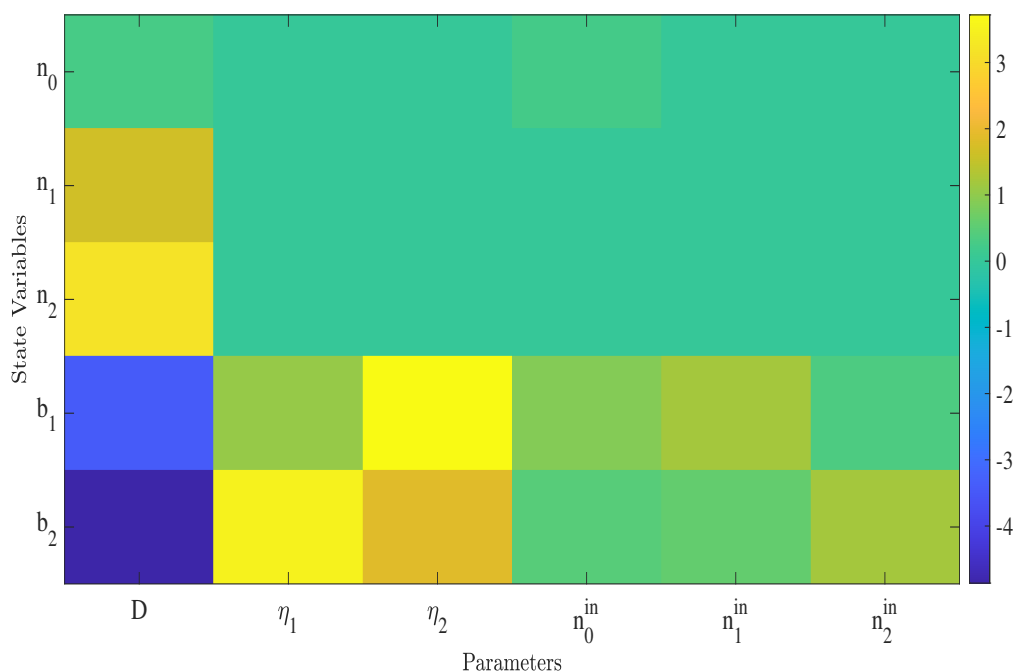

Figure 18. Local sensitivity of equilibrium components to parameters.

The figures collectively demonstrate:

- Higher D or mutualism coefficients can destabilize coexistence.
- n_1^{in} and n_2^{in} are pivotal for sustaining respective species.
- Guides experimental design by ranking parameter impacts.

These results align with the theoretical stability conditions (e.g., $f_i > D$ for persistence) and highlight the model's robustness in predicting chemostat dynamics.

6. Optimal control problem formulation

We consider the chemostat model (2.2) with the dilution rate, $D(t)$ as a time-dependent control variable. The goal is to maximize the total bacterial biomass over a fixed time horizon $[0, T]$ while minimizing the input nutrient cost.

6.1. State equations

Assume that f_1 and f_2 are globally Lipschitz with Lipschitz constants L_1 and L_2, respectively, with upper bounds $\bar{f}_1 = \sup\limits_{n_1 > 0} f_1(n_1)$ and $\bar{f}_2 = \sup\limits_{n_2 > 0} f_2(n_2)$, respectively. Assume also that the dilution

rate, D, is variable on the time interval $[0, T]$, where $T > 0$ is a constant. Therefore, the controlled system is:

$$
\begin{aligned}
\dot{n}_0 &= D(t)(n_0^{in} - n_0) - \delta u n_0 \\
\dot{n}_1 &= D(t)(n_1^{in} - n_1) + \delta u n_0 - f_1(n_1)b_1 + \eta_2 f_2(n_2)b_2 \\
\dot{n}_2 &= D(t)(n_2^{in} - n_2) - f_2(n_2)b_2 + \eta_1 f_1(n_1)b_1 \\
\dot{b}_1 &= (f_1(n_1) - D(t))b_1 \\
\dot{b}_2 &= (f_2(n_2) - D(t))b_2.
\end{aligned}
\tag{6.1}
$$

For $Z = (n_0, n_1, n_2, b_1, b_2)^t$, the model (6.1) can be written as follows

$$
\dot{Z} = AZ + \sigma_1(Z) = \sigma_2(Z)
\tag{6.2}
$$

with $A = \begin{pmatrix} -D & 0 & 0 & 0 & 0 \\ 0 & -D & 0 & 0 & 0 \\ 0 & 0 & -D & 0 & 0 \\ 0 & 0 & 0 & -D & 0 \\ 0 & 0 & 0 & 0 & -D \end{pmatrix}$ and $\sigma_1(Z) = \begin{pmatrix} Dn_0^{in} - \delta u n_0 \\ Dn_1^{in} + \delta u n_0 - f_1(n_1)b_1 + \eta_2 f_2(n_2)b_2 \\ Dn_2^{in} - f_2(n_2)b_2 + \eta_1 f_1(n_1)b_1 \\ f_1(n_1)b_1 \\ f_2(n_2)b_2 \end{pmatrix}$.

Theorem 5. σ_2 *is a uniformly Lipschitz function.*

Proof. The following provide simple calculus prove that σ_1 is uniformly Lipschitz:

$$
\begin{aligned}
\left\| \sigma_1(Z') - \sigma_1(Z) \right\|_1 &= \left| \delta u n_0' - \delta u n_0 \right| + \left| \delta u n_0' - f_1(n_1')b_1' + \eta_2 f_2(n_2')b_2' - \delta u n_0 + f_1(n_1)b_1 - \eta_2 f_2(n_2)b_2 \right| \\
&\quad + \left| -f_2(n_2')b_2' + \eta_1 f_1(n_1')b_1' + f_2(n_2)b_2 - \eta_1 f_1(n_1)b_1 \right| \\
&\quad + \left| f_1(n_1')b_1' - f_1(n_1)b_1 \right| + \left| f_2(n_2')b_2' - f_2(n_2)b_2 \right| \\
&\leq 2\delta u \left| n_0' - n_0 \right| + 3 \left| f_1(n_1')b_1' - f_1(n_1)b_1 \right| + 3 \left| f_2(n_2')b_2' - f_2(n_2)b_2 \right| \\
&= 2\delta u \left| n_0' - n_0 \right| + 3 \left| f_1(n_1')b_1' - f_1(n_1)b_1' + f_1(n_1)(b_1' - b_1) \right| \\
&\quad + 3 \left| f_2(n_2')b_2' - f_2(n_2)b_2' + f_2(n_2)(b_2' - b_2) \right| \\
&\leq 2\delta u \left| n_0' - n_0 \right| + 3L_1 \frac{n_0^{in} + n_1^{in} + n_2^{in}}{1 - \eta_1} \left| n_1' - n_1 \right| + \bar{f}_1 \left| b_1' - b_1 \right| \\
&\quad + 3L_2 \frac{n_0^{in} + n_1^{in} + n_2^{in}}{1 - \eta_2} \left| n_2' - n_2 \right| + \bar{f}_2 \left| b_2' - b_2 \right| \\
&\leq L \left\| Z' - Z \right\|_1,
\end{aligned}
$$

where $L = \max\left(2\delta u, 3L_1 \dfrac{n_0^{in} + n_1^{in} + n_2^{in}}{1 - \eta_1}, \bar{f}_1, 3L_2 \dfrac{n_0^{in} + n_1^{in} + n_2^{in}}{1 - \eta_2}, \bar{f}_2 \right)$. Furthermore, the matrix A verifies

$$
\left\| AZ' - AZ \right\|_1 = D \left\| Z' - Z \right\|_1,
$$

thus,

$$
\left\| \sigma_2(Z') - \sigma_2(Z) \right\|_1 \leq \delta \left\| Z' - Z \right\|_1,
$$

with $\delta = \max(L, D)$ and thus, the continuous function, σ is uniformly Lipschitz. $\qquad\square$

One can conclude easily that the dynamics (6.2) admits a unique solution.

6.2. Objective functional

We define two competing objectives where the aim is to maximize total biomass inside the chemostat and minimize nutrient input and the cost:

(1) Maximize total biomass: $J_1 = \int_0^T (b_1(t) + b_2(t)) \, dt$.

(2) Minimize nutrient input: $J_2 = \int_0^T D(t)(n_0^{in} + n_1^{in} + n_2^{in}) \, dt$.

The combined objective is:

$$J(D) = \alpha J_1 - (1 - \alpha)J_2 \quad \text{with} \quad \alpha \in [0, 1]$$

where α balances biomass production against resource cost.

6.3. Pontryagin's maximum principle

We apply Pontryagin's maximum principle [24,25,29] to derive necessary conditions for optimality. The Hamiltonian is:

$$\begin{aligned}
\mathscr{H} = {} & \alpha(b_1 + b_2) - (1 - \alpha)D(n_0^{in} + n_1^{in} + n_2^{in}) \\
& + \lambda_0[D(n_0^{in} - n_0) - \delta u n_0] \\
& + \lambda_1[D(n_1^{in} - n_1) + \delta u n_0 - f_1(n_1)b_1 + \eta_2 f_2(n_2)b_2] \\
& + \lambda_2[D(n_2^{in} - n_2) - f_2(n_2)b_2 + \eta_1 f_1(n_1)b_1] \\
& + \lambda_3[(f_1(n_1) - D)b_1] \\
& + \lambda_4[(f_2(n_2) - D)b_2].
\end{aligned}$$

The adjoint system is derived from the Hamiltonian $\mathscr{H}$ using the relation $\dot{\lambda}_i = -\dfrac{\partial \mathscr{H}}{\partial x_i}$, where x_i represents the state variables $(n_0, n_1, n_2, b_1, b_2)$. The adjoint equations are given by:

$$\begin{cases}
\dot{\lambda}_0 & = \lambda_0(D + \delta u) - \lambda_1 \delta u, \\
\dot{\lambda}_1 & = \lambda_1(D + f_1'(n_1)b_1) - \lambda_2 \eta_1 f_1'(n_1)b_1 - \lambda_3 f_1'(n_1)b_1, \\
\dot{\lambda}_2 & = -\lambda_1 \eta_2 f_2'(n_2)b_2 + \lambda_2(D + f_2'(n_2)b_2) - \lambda_4 f_2'(n_2)b_2, \\
\dot{\lambda}_3 & = -\alpha + \lambda_1 f_1(n_1) - \lambda_2 \eta_1 f_1(n_1) - \lambda_3(f_1(n_1) - D), \\
\dot{\lambda}_4 & = -\alpha - \lambda_1 \eta_2 f_2(n_2) + \lambda_2 f_2(n_2) - \lambda_4(f_2(n_2) - D).
\end{cases}$$

The explanation of the adjoint system terms is given as follows :

- $\lambda_0(D + \delta u)$ reflects the derivative of $\mathscr{H}$ w.r.t. n_0 in the first state equation.
- $-\lambda_1 \delta u$ reflects the coupling term $\delta u n_0$ in the second state equation.
- $\lambda_1(D + f_1'(n_1)b_1)$ reflects the derivative of $\mathscr{H}$ w.r.t. n_1 in the second state equation.
- $-\lambda_2 \eta_1 f_1'(n_1)b_1$ and $-\lambda_3 f_1'(n_1)b_1$ reflects the mutualistic interactions and growth rate of b_1.
- $-\lambda_1 \eta_2 f_2'(n_2)b_2$ reflects the mutualistic contribution of b_2 to n_1.
- $\lambda_2(D + f_2'(n_2)b_2)$ reflects the derivative of $\mathscr{H}$ w.r.t. n_2 in the third state equation.

- $-\lambda_4 f_2'(n_2)b_2$ reflects the growth rate of b_2.
- $-\alpha$ reflects the objective functional $J_1 = \int_0^T (b_1 + b_2)\, dt$.
- Remaining terms reflect the interactions and growth dynamics of b_1.
- $-\alpha$ reflects the objective functional J_1.
- Remaining terms: Interactions and growth dynamics of b_2.

This adjoint system is solved backward in time with terminal conditions $\lambda_i(T) = 0$ for $i = 0,1,2,3,4$, as is typical in optimal control problems. The solution of this system, along with the state equations, is used to characterize the optimal control $D^*(t)$.

6.4. Optimal control characterization

The optimal control $D^*(t)$ satisfies:

$$D^* = \arg\max_{D_{\min} \leq D \leq D_{\max}} \mathcal{H}.$$

This leads to a bang-singular-bang control structure.

6.5. Numerical scheme for optimal control

The optimal control problem is solved using a forward-backward sweep method (see Algorithm 1) with the following steps:

State equations (forward system)

The state variables $(n_0, n_1, n_2, b_1, b_2)$ are solved forward in time using the ODEs:

$$
\begin{cases}
\dot{n}_0 = D(t)(n_0^{in} - n_0) - \delta u n_0, \\
\dot{n}_1 = D(t)(n_1^{in} - n_1) + \delta u n_0 - f_1(n_1)b_1 + \eta_2 f_2(n_2)b_2, \\
\dot{n}_2 = D(t)(n_2^{in} - n_2) - f_2(n_2)b_2 + \eta_1 f_1(n_1)b_1, \\
\dot{b}_1 = (f_1(n_1) - D(t))b_1, \\
\dot{b}_2 = (f_2(n_2) - D(t))b_2,
\end{cases}
$$

with initial conditions $n_0(0), n_1(0), n_2(0), b_1(0),$ and $b_2(0)$.

Adjoint equations (backward system)

The adjoint variables $(\lambda_0, \lambda_1, \lambda_2, \lambda_3, \lambda_4)$ are solved backward in time:

$$
\begin{cases}
\dot{\lambda}_0 = \lambda_0(D + \delta u) - \lambda_1 \delta u, \\
\dot{\lambda}_1 = \lambda_1(D + f_1'(n_1)b_1) - \lambda_2 \eta_1 f_1'(n_1)b_1 - \lambda_3 f_1'(n_1)b_1, \\
\dot{\lambda}_2 = -\lambda_1 \eta_2 f_2'(n_2)b_2 + \lambda_2(D + f_2'(n_2)b_2) - \lambda_4 f_2'(n_2)b_2, \\
\dot{\lambda}_3 = -\alpha + \lambda_1 f_1(n_1) - \lambda_2 \eta_1 f_1(n_1) - \lambda_3(f_1(n_1) - D), \\
\dot{\lambda}_4 = -\alpha - \lambda_1 \eta_2 f_2(n_2) + \lambda_2 f_2(n_2) - \lambda_4(f_2(n_2) - D),
\end{cases}
$$

with terminal conditions $\lambda_i(T) = 0$ for $i = 0, \ldots, 4$.

Optimal control characterization

The control $D(t)$ is updated using the Hamiltonian maximization condition:

$$D^*(t) = \begin{cases} D_{\min} & \text{if } \dfrac{\partial \mathscr{H}}{\partial D} < 0, \\[2mm] D_{\max} & \text{if } \dfrac{\partial \mathscr{H}}{\partial D} > 0, \\[2mm] D_{\text{sing}} & \text{otherwise}, \end{cases}$$

where D_{sing} is the singular control obtained by solving $\dfrac{\partial \mathscr{H}}{\partial D} = 0$.

6.6. Numerical implementation

6.6.1. Discretization

(1) **Time Grid**: Divide $[0, T]$ into N intervals with step size $\Delta t = T/N$.

(2) **Forward Sweep**:

- Use the 4th-order Runge-Kutta (RK4) method to solve state equations.
- Initialize with $n_0(0), n_1(0), n_2(0), b_1(0), b_2(0)$.

(3) **Backward Sweep**:

- Solve adjoint equations using RK4 with terminal conditions $\lambda_i(T) = 0$.
- Store state variables from the forward sweep for evaluation.

(4) **Control Update**:

- Compute $D^*(t)$ at each time step using the Hamiltonian gradient.
- Apply projection to enforce $D_{\min} \leq D(t) \leq D_{\max}$.

6.6.2. Convergence criterion

The algorithm iterates until:

$$\max \left(\|D_{\text{new}} - D_{\text{old}}\|_\infty, \|\mathbf{x}_{\text{new}} - \mathbf{x}_{\text{old}}\|_\infty \right) < \varepsilon,$$

where ε is a tolerance (e.g., 10^{-6}).

6.6.3. Algorithm details

- **State Equations (F):** Solved forward in time using RK4 with current control estimate
- **Adjoint Equations (G):** Solved backward in time using RK4 with terminal conditions $\boldsymbol{\lambda}(T) = \mathbf{0}$
- **Control Update:** Gradient ascent with projection to enforce $D \in [D_{\min}, D_{\max}]$
- **Convergence:** Measured by maximum change in control between iterations
- **RK4 Implementation:** Fourth-order Runge-Kutta ensures numerical stability

Remark that

- The RK4 method ensures stability for stiff systems.
- The control update may require gradient-based optimization if singular arcs exist.
- Parallelization can accelerate the forward-backward sweeps for large N.

Algorithm 1 Forward-Backward Sweep Method for Chemostat Optimal Control

---

1: **Input:**
2:   Model parameters: $D_{\min}, D_{\max}, \alpha, \eta_1, \eta_2, \delta u, n_0^{in}, n_1^{in}, n_2^{in}$
3:   Numerical parameters: $T, N, \text{tol}, \text{max\_iter}$
4:   Initial conditions: $\mathbf{x}_0 = [n_0(0), n_1(0), n_2(0), b_1(0), b_2(0)]^T$
5:   Growth rate functions: $f_1(n_1), f_2(n_2), f_1'(n_1), f_2'(n_2)$
6: **Initialize:**
7:   Time grid: $t_k = k\Delta t$ for $k = 0, \ldots, N$ with $\Delta t = T/N$
8:   State variables: $\mathbf{x}^{(0)} \leftarrow \mathbf{x}_0$
9:   Adjoint variables: $\boldsymbol{\lambda}^{(0)} \leftarrow \mathbf{0}$
10:   Control: $D^{(0)}(t_k) \leftarrow D_{\min}$ for all k
11:   Iteration counter: $i \leftarrow 0$
12: **while** $i < \text{max\_iter}$ **do**
13:   $i \leftarrow i + 1$
14:   **1. Forward Sweep (State Equations):**
15:   **for** $k = 0$ to $N - 1$ **do**
16:     Compute RK4 steps:
17:     $\mathbf{k}_1 \leftarrow \Delta t\, \mathbf{F}(\mathbf{x}_k^{(i)}, D_k^{(i-1)})$
18:     $\mathbf{k}_2 \leftarrow \Delta t\, \mathbf{F}(\mathbf{x}_k^{(i)} + \frac{1}{2}\mathbf{k}_1, D_k^{(i-1)})$
19:     $\mathbf{k}_3 \leftarrow \Delta t\, \mathbf{F}(\mathbf{x}_k^{(i)} + \frac{1}{2}\mathbf{k}_2, D_k^{(i-1)})$
20:     $\mathbf{k}_4 \leftarrow \Delta t\, \mathbf{F}(\mathbf{x}_k^{(i)} + \mathbf{k}_3, D_k^{(i-1)})$
21:     $\mathbf{x}_{k+1}^{(i)} \leftarrow \mathbf{x}_k^{(i)} + \frac{1}{6}(\mathbf{k}_1 + 2\mathbf{k}_2 + 2\mathbf{k}_3 + \mathbf{k}_4)$
22:   **end for**
23:   **2. Backward Sweep (Adjoint Equations):**
24:   **for** $k = N$ downto 1 **do**
25:     Compute RK4 steps:
26:     $\mathbf{l}_1 \leftarrow -\Delta t\, \mathbf{G}(\boldsymbol{\lambda}_k^{(i)}, \mathbf{x}_{k-1}^{(i)}, D_{k-1}^{(i-1)})$
27:     $\mathbf{l}_2 \leftarrow -\Delta t\, \mathbf{G}(\boldsymbol{\lambda}_k^{(i)} + \frac{1}{2}\mathbf{l}_1, \mathbf{x}_{k-1}^{(i)}, D_{k-1}^{(i-1)})$
28:     $\mathbf{l}_3 \leftarrow -\Delta t\, \mathbf{G}(\boldsymbol{\lambda}_k^{(i)} + \frac{1}{2}\mathbf{l}_2, \mathbf{x}_{k-1}^{(i)}, D_{k-1}^{(i-1)})$
29:     $\mathbf{l}_4 \leftarrow -\Delta t\, \mathbf{G}(\boldsymbol{\lambda}_k^{(i)} + \mathbf{l}_3, \mathbf{x}_{k-1}^{(i)}, D_{k-1}^{(i-1)})$
30:     $\boldsymbol{\lambda}_{k-1}^{(i)} \leftarrow \boldsymbol{\lambda}_k^{(i)} + \frac{1}{6}(\mathbf{l}_1 + 2\mathbf{l}_2 + 2\mathbf{l}_3 + \mathbf{l}_4)$
31:   **end for**

32:    **3. Control Update:**

33:    **for** $k = 0$ to N **do**

34:       Compute Hamiltonian gradient:

35:       $\dfrac{\partial H}{\partial D} \leftarrow -(1-\alpha)(n_0^{in} + n_1^{in} + n_2^{in}) + \lambda_0^{(i)}(n_0^{in} - n_0^{(i)})$

36:       $+\lambda_1^{(i)}(n_1^{in} - n_1^{(i)}) + \lambda_2^{(i)}(n_2^{in} - n_2^{(i)}) - \lambda_3^{(i)} b_1^{(i)} - \lambda_4^{(i)} b_2^{(i)}$

37:       Update control:

38:       $D_k^{(i)} \leftarrow \text{proj}_{[D_{\min},D_{\max}]}\left(D_k^{(i-1)} + \gamma\dfrac{\partial H}{\partial D}\right)$

39:    **end for**

40:    **4. Check Convergence:**

41:    error $\leftarrow \max_k |D_k^{(i)} - D_k^{(i-1)}|$

42:    **if** error $<$ tol **then**

43:       **break**

44:    **end if**

45: **end while**

46: **Output:**

47:    Optimal control trajectory: $D^*(t_k)$

48:    State trajectories: $\mathbf{x}^*(t_k)$

49:    Adjoint trajectories: $\boldsymbol{\lambda}^*(t_k)$

50: **where:**

51: $\mathbf{F}(\mathbf{x},D) = \begin{cases} D(n_0^{in} - n_0) - \delta u n_0 \\ D(n_1^{in} - n_1) + \delta u n_0 - f_1(n_1)b_1 + \eta_2 f_2(n_2)b_2 \\ D(n_2^{in} - n_2) - f_2(n_2)b_2 + \eta_1 f_1(n_1)b_1 \\ (f_1(n_1) - D)b_1 \\ (f_2(n_2) - D)b_2 \end{cases}$

52: $\mathbf{G}(\boldsymbol{\lambda},\mathbf{x},D) = \begin{cases} \lambda_0(D + \delta u) - \lambda_1 \delta u \\ \lambda_1(D + f_1'(n_1)b_1) - \lambda_2 \eta_1 f_1'(n_1)b_1 - \lambda_3 f_1'(n_1)b_1 \\ -\lambda_1 \eta_2 f_2'(n_2)b_2 + \lambda_2(D + f_2'(n_2)b_2) - \lambda_4 f_2'(n_2)b_2 \\ -\alpha + \lambda_1 f_1(n_1) - \lambda_2 \eta_1 f_1(n_1) - \lambda_3(f_1(n_1) - D) \\ -\alpha - \lambda_1 \eta_2 f_2(n_2) + \lambda_2 f_2(n_2) - \lambda_4(f_2(n_2) - D) \end{cases}$

We perform numerical results on a system that uses Monod functions to express growth rates:

$$f_1(n_2) = \frac{f_1^{max} n_2}{\kappa_1 + n_2} \text{ and } f_2(n_2) = \frac{f_2^{max} n_2}{\kappa_2 + n_2}$$

where κ_1 and κ_2 are Monod constants, and f_1^{max} and f_2^{max} are the maximum growth rates of bacteria 1 and bacteria 2, respectively. One can readily check that functions f_1 and f_2 satisfy Assumption 1. Some parameters are provided in Table 1.

Figure 19 illustrates the dynamics of nutrient concentrations (n_0, n_1, n_2) and bacterial biomass concentrations (b_1, b_2) under the influence of an optimally controlled dilution rate $D(t)$. The figure likely consists of multiple subplots showing the trajectories of these variables over time. The dilution rate $D(t)$ is dynamically adjusted to balance the competing objectives of maximizing total biomass $(b_1 + b_2)$ and minimizing nutrient input costs. The trajectory of $D(t)$ may exhibit an initial high phase to rapidly stabilize the system, followed by a decline to a steady-state value that sustains coexistence. Alternatively, it may show a bang-singular-bang structure, switching between bounds $(D_{min}$ and $D_{max})$ and intermediate values based on the Hamiltonian gradient. Initially high due to input, n_0 decreases as it is converted into soluble forms (n_1 or n_2) or or washed out. The steady-state value reflects a balance between input, conversion, and dilution. The soluble nutrients are consumed by bacteria and recycled through mutualism. Their concentrations stabilize at levels where bacterial uptake matches supply and recycling rates. Peaks or dips may correspond to phases of high bacterial activity or dilution adjustments. Both species grow until their growth rates $(f_1(n_1), f_2(n_2))$ are balanced by the dilution rate $D(t)$. Mutualism (η_1, η_2) enables coexistence, as each species benefits from the other's nutrient recycling. The biomass trajectories show logistic-like growth, reaching steady states where production matches washout. The relative abundance of b_1 and b_2 depends on their growth efficiencies and mutualistic strengths. The stable coexistence of b_1 and b_2 is achieved under optimal control, validating the theoretical analysis of E_{12}. Higher $D(t)$ reduces biomass (increased washout) but lowers nutrient costs, while lower $D(t)$ favors biomass accumulation at higher resource costs. The optimal $D(t)$ strikes a balance dictated by the weight α. The trajectories are influenced by mutualism coefficients (η_1, η_2) and growth kinetics $(f_1(n_1), f_2(n_2))$. For example, stronger mutualism (higher η_i) may elevate steady-state biomass. The results suggest that time-varying dilution strategies outperform constant rates in maintaining coexistence and optimizing objectives. The model can guide bioreactor operations by identifying critical parameters (e.g., η_i, input concentrations) for desired outcomes. Therefore, we conclude that Figure 19 demonstrates how optimal control of the dilution rate enables stable coexistence of mutualistic bacteria while efficiently utilizing nutrients. The trajectories align with the theoretical stability analysis and highlight the interplay between system dynamics and control objectives. Some key findings from the provided numerical simulations are summarized as follows: For $\alpha \approx 1$ (biomass maximization), optimal $D(t)$ starts high to quickly reach steady-state, then decreases to maintain coexistence. For $\alpha \approx 0$ (resource minimization), $D(t)$ remains near the minimum required to prevent washout. Mutualism parameters η_1, η_2 significantly affect the optimal control trajectory. The optimal control framework provides: Quantitative trade-offs between biomass production and resource use. Time-varying dilution strategies superior to constant D. Sensitivity analysis of control to mutualism parameters.
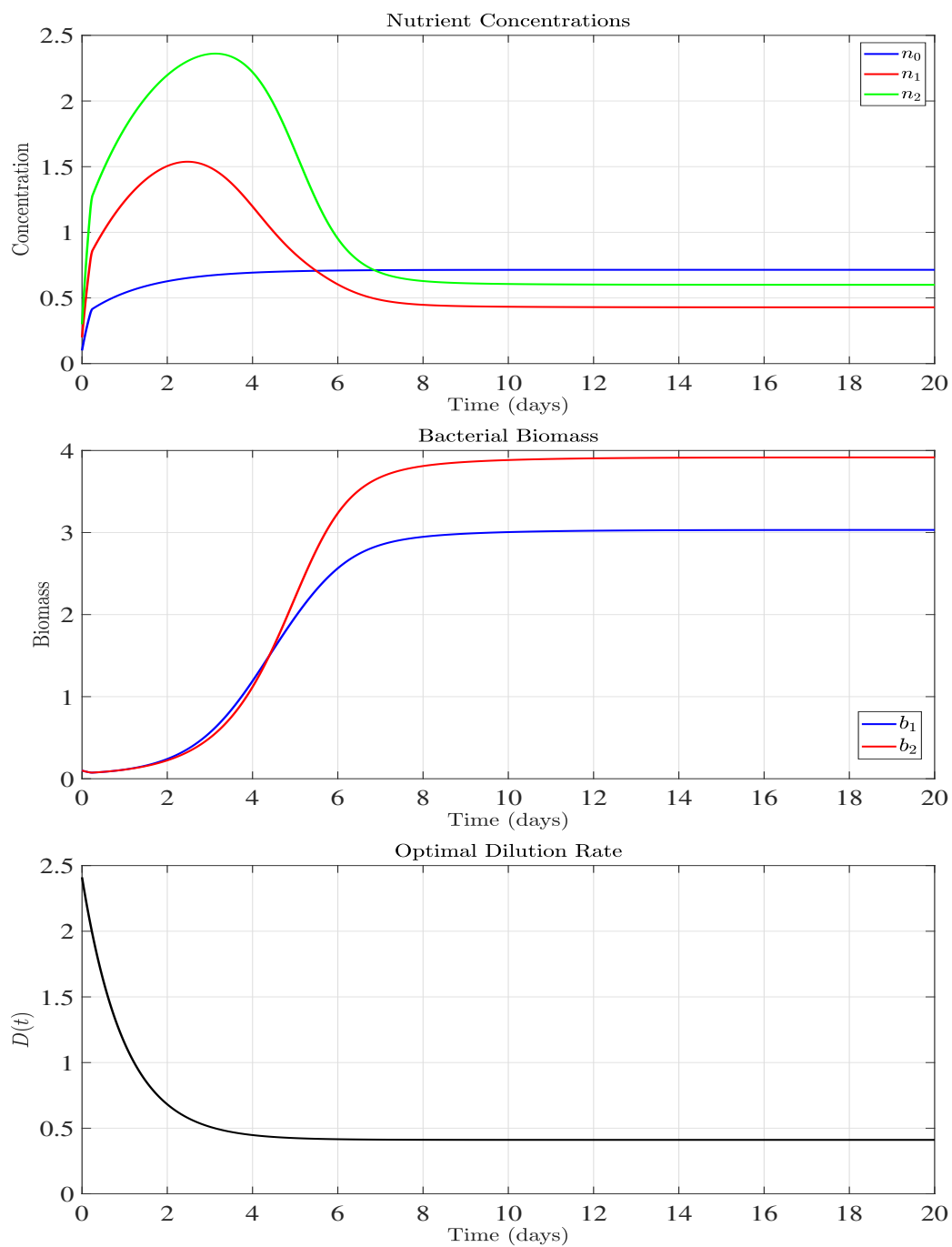
Figure 19. Optimal nutrient and biomass concentrations corresponding to the optimal dilution rate.

Table 1. Parameters for numerical simulation

Parameter	Description	Value
T	Final time	10 days
N	Time steps	1000
$D_{\min}, D_{\max}$	Control bounds	$[0.1, 2.0]\,\text{day}^{-1}$
α	Trade-off weight	0.7
η_1, η_2	Mutualism coefficients	0.5, 0.3

7. Conclusions

We presented a comprehensive analysis of a chemostat model involving two mutualistic bacterial species competing for nutrients, with the added complexity of leachate recycling for one substrate. By reducing the original five-dimensional system to a more tractable three-dimensional form, we identified and analyzed four key equilibrium points: The washout equilibrium (E_0), single-species equilibria (E_2 and E_2), and the coexistence equilibrium (E_{12}). Through local stability analysis, we established conditions under which each equilibrium is stable or unstable, demonstrating that the coexistence equilibrium E_{12} is locally asymptotically stable under biologically realistic assumptions. By using the principle of uniform persistence applied to the reduced system, we proved that the two competing bacteria can coexist. Numerical simulations validated these theoretical findings, illustrating transitions between equilibria and the influence of key parameters on system dynamics. A sensitivity analysis revealed that the dilution rate, mutualism coefficients, and nutrient input concentrations significantly impact the system's behavior. Optimal control techniques were then applied to determine the best dilution strategy for maximizing biomass production while minimizing nutrient costs. The forward-backward sweep method provided numerical solutions, demonstrating that time-varying dilution rates can enhance system performance compared to constant-rate operation.

While this study provides a robust theoretical and numerical framework, it is subject to some limitations. The use of Monod kinetics may oversimplify complex microbial growth dynamics, and the deterministic model does not capture environmental fluctuations or stochastic effects. Furthermore, the focus on two bacterial species limits the applicability to more diverse microbial communities. In the future, researchers should aim at experimental validation of model predictions, extension to stochastic frameworks to incorporate random environmental variability, and generalization to multi-species systems to better represent natural and engineered ecosystems. Other extensions could further enhance its applicability:

- Incorporating random fluctuations in nutrient supply or bacterial growth rates could improve model realism. Multi-Species Mutualism: Extending the model to include additional species or more complex interaction networks would better reflect natural microbial communities.
- Testing the model predictions in laboratory bioreactors would strengthen its practical relevance.
- Exploring Pareto-optimal strategies for balancing competing objectives (e.g., biomass yield vs. energy efficiency) could refine control policies.

In summary, this work bridges theoretical ecology and bioreactor engineering, offering insights into microbial coexistence and optimization strategies for engineered systems. The findings contribute to

the broader understanding of mutualistic interactions in continuous cultures and provide a foundation for future research in microbial ecology and bioprocess control.

Author contributions

All authors make equal contributions to the research work. All authors have read and agreed to the published version of the manuscript.

Use of AI tools declaration

The authors declare they have not used Artificial Intelligence (AI) tools in the creation of this article.

Acknowledgments

Funding

Conflict of interest

All the authors declare no conflicts of interest.

References

1. H. L. Smith, P. Waltman, *The theory of the chemostat*, Dynamics of microbial competition, **13** (1995), Cambridge Studies in Mathematical Biology, Cambridge University Press.

2. M. El Hajji, J. Harmand, H. Chaker, C. Lobry, Association between competition and obligate mutualism in a chemostat, *J. Biol. Dynam.*, **3** (2009), 635–647. https://doi.org/10.1080/17513750902915978

3. A. H. Albargi, M. El Hajji, Mathematical analysis of a two-tiered microbial food-web model for the anaerobic digestion process, *Math. Biosci. Eng.*, **20** (2023), 6591–6611. https://doi.org/10.3934/mbe.2023283

4. A. A. Alsolami, M. El Hajji, Mathematical analysis of a bacterial competition in a continuous reactor in the presence of a virus, *Mathematics*, **11** (2023), 883. https://doi.org/10.3390/math11040883

5. L. Margulis, Symbiosis and evolution, *Sci. Am.*, **225** (1971), 48–61. https://doi.org/10.1038/scientificamerican0871-48

6. A. M. Dean, A simple model of mutualism, *Am. Nat.*, **121** (1983), 409–417. https://doi.org/10.1086/284069

7. S. Vet, S. de Buyl, K. Faust, J. Danckaert, D. Gonze, L. Gelens, Bistability in a system of two species interacting through mutualism as well as competition: Chemostat vs. lotka-volterra equations, *PLoS One*, **13** (2018), 1–15. https://doi.org/10.1371/journal.pone.0197462

8. Y. Daoud, N. Abdellatif, T. Sari, J. Harmand, Steady state analysis of a syntrophic model: The effect of a new input substrate concentration, *Math. Model. Nat. Phenom.*, **13** (2018), 31. https://doi.org/10.1051/mmnp/2018037

9. R. Fekih-Salem, Y. Daoud, N. Abdellatif, T. Sari, A mathematical model of anaerobic digestion with syntrophic relationship, substrate inhibition and distinct removal rates, *SIAM J. Appl. Dyn. Syst.*, **20** (2020), 1621–1654. https://doi.org/10.1137/20M1376480

10. M. El Hajji, F. Mazenc, J. Harmand, A mathematical study of a syntrophic relationship of a model of anaerobic digestion process, *Math. Biosci. Eng.*, **7** (2010), 641–656. https://doi.org/10.3934/mbe.2010.7.641

11. T. Sari, M. El Hajji, J. Harmand, The mathematical analysis of a syntrophic relationship between two microbial species in a chemostat, *Math. Biosci. Eng.*, **9** (2012), 627–645. https://doi.org/10.3934/mbe.2012.9.627

12. X. Zhao, L. Li, D. Wu, T. Xiao, Y. Ma, X. Peng, Modified anaerobic digestion model no. 1 for modeling methane production from food waste in batch and semi-continuous anaerobic digestions, *Bioresource Technol.*, **271** (2019), 109–117. https://doi.org/10.1016/j.biortech.2018.09.091

13. T. Sari, J. Harmand, A model of a syntrophic relationship between two microbial species in a chemostat including maintenance, *Math. Biosci.*, **275** (2016), 1–9. https://doi.org/10.1016/j.mbs.2016.02.008

14. H. H. Almuashi, N. A. Almuallem, M. El Hajji, The effect of leachate recycling on the dynamics of two competing bacteria with an obligate one-way beneficial relationship in a chemostat, *Mathematics*, **12** (2024), 23. https://doi.org/10.3390/math12233819

15. N. A. Almuallem, M. El Hajji, How can viruses affect the growth of zooplankton on phytoplankton in a chemostat?, *Mathematics*, **13** (2025), 7. https://doi.org/10.3390/math13071192

16. F. A. Al Najim, M. El Hajji, B. S. Alshammari, A microbial food web dynamics under the influence of leachate recirculation, *Mathematics*, **13** (2025), 13. https://doi.org/10.3390/math13132146

17. J. D. Murray, *Continuous models for interacting populations*, Berlin, Heidelberg: Springer Berlin Heidelberg, 1993, 63–94. https://doi.org/10.1007/978-3-662-08539-4_3

18. N. W. Smith, P. R. Shorten, E. Altermann, N. C. Roy, W. C. McNabb, The classification and evolution of bacterial cross-feeding, *Front. Ecol. Evol.*, **7** (2019). https://doi.org/10.3389/fevo.2019.00153

19. J. C. Moore, The influence of microarthropods on symbiotic and non-symbiotic mutualism in detrital-based below-ground food webs, *Agr. Ecosyst. Environ.*, **24** (1988), 147–159. https://doi.org/10.1016/0167-8809(88)90062-X

20. F. Abiusi, R. H. Wijffels, M. Janssen, Doubling of microalgae productivity by oxygen balanced mixotrophy, *ACS Sustain. Chem. Eng.*, **8** (2020), 6065–6074. https://doi.org/10.1021/acssuschemeng.0c00990

21. M. Bisi, M. Groppi, G. Martaló, R. Travaglini, Optimal control of leachate recirculation for anaerobic processes in landfills, *Discrete Cont. Dyn.-B*, **26** (2021), 2957–2976. https://doi.org/10.3934/dcdsb.2020215

22. O. Laraj, N. El Khattabi, *A. Rapaport, Mathematical model of anaerobic digestion with leachate recirculation*, in CARI 2022, (Tunis, Tunisia), Oct 2022.

23. J. LaSalle, *The stability of dynamical systems*, SIAM, 1976.

24. L. S. Pontryagin, V. G. Boltyanskii, R. V. Gamkrelidze, E. F. Mishchenko, K. N. Trirogoff, L. W. Neustadt, *The mathematical theory of optimal processes*, CRC Press, 2000.

25. S. Lenhart, J. T. Workman, *Optimal control applied to biological models*, Chapman and Hall, 2007. https://doi.org/10.1201/9781420011418

26. Y. Guo, T. Li, Fractional-order modeling and optimal control of a new online game addiction model based on real data, *Commun. Nonlinear Sci.*, **121** (2023), 107221. https://doi.org/10.1016/j.cnsns.2023.107221

27. Y. Guo, T. Li, Modeling the competitive transmission of the omicron strain and delta strain of covid-19, *J. Math. Anal. Appl.*, **526** (2023), 127283. https://doi.org/10.1016/j.jmaa.2023.127283

28. T. Li, Y. Guo, Modeling and optimal control of mutated covid-19 (delta strain) with imperfect vaccination, *Chaos Soliton. Fract.*, **156** (2022), 111825. https://doi.org/10.1016/j.chaos.2022.111825

29. W. Fleming, R. Rishel, *Deterministic and stochastic optimal control*, Springer Verlag, New York, 1975. https://doi.org/10.2307/2344363

30. J. C. Arceo, O. Bernard, J.-L. Gouzé, *Bacteria mutualism in a chemostat: Analysis and optimization with interval detector*, in 2022 IEEE 61st Conference on Decision and Control (CDC), 2022, 3225–3230.

31. M. El Hajji, Mathematical modeling for anaerobic digestion under the influence of leachate recirculation, *AIMS Math.*, **8** (2023), 30287–30312. https://doi.org/10.3934/math.20231547

32. H. R. Thieme, Convergence results and a Poincaré-Bendixson trichotomy for asymptotically autonomous differential equations, *J. Math. Biol.*, **30** (1992), 755–763. https://doi.org/10.1007/BF00173267

33. M. El Hajji, How can inter-specific interferences explain coexistence or confirm the competitive exclusion principle in a chemostat, *Int. J. Biomath.*, **11** (2018), 1850111. https://doi.org/10.1142/S1793524518501115

34. S. Sobieszek, M. J. Wade, G. S. K. Wolkowicz, Rich dynamics of a three-tiered anaerobic food-web in a chemostat with multiple substrate inflow, *Math. Biosci. Eng.*, **17** (2020), 7045–7073. https://doi.org/10.3934/mbe.2020363